Geophys. J. Int. (1990) **103**, 731–754

Determination of seismic wavefields in arbitrarily continuously layered media using the modified Cagniard method

M. D. Verweij and A. T. de Hoop

Laboratory of Electromagnetic Research, Department of Electrical Engineering, Delft University of Technology, PO Box 5031, 2600 GA Delft, The Netherlands

Accepted 1990 July 13. Received 1990 July 12; in original form 1989 June 30

SUMMARY

In this paper we investigate a combination of the WKBJ iterative solution and the modified Cagniard method (also called the Cagniard–De Hoop method) that, in principle, yields a theoretically exact space–time domain solution for the 3-D seimic wave propagation problem in continuously layered media. Owing to the application of the Laplace transformation with a real and positive transformation parameter with respect to the time coordinate, the convergence of the iterative scheme for an arbitrary configuration, both before and after the transformation back to the space–time domain, is guaranteed. In constrast to the standard frequency-domain analysis, difficulties due to turning points can be avoided. This is due to the fact that along the original integration paths of the inverse transformations the propagation coefficient never becomes zero, while during deformation of the integration contour a point that yields a zero propagation coefficient can be dealt with by properly going around it. The inverse transformation procedure is demonstrated for the direct wave and the wave due to single partial reflections in a medium. Numerical results for these components are presented.

Key words: continuously layered configurations, modified Cagniard method, WKBJ iterative solution.

1 INTRODUCTION

In this paper we theoretically investigate the influence of vertical inhomogeneity of a medium on the propagation of seismic waves. To solve a wave propagation problem, we could apply a brute-force approach and solve directly the basic system of differential equations that describes the problem, e.g., by finite-elements or finite-difference methods. For a general configuration this is often the only way to obtain a solution. In this paper we investigate the more specific case of horizontally layered configurations. Having this specific structure, special methods are available, which are numerically more efficient than the brute-force approach, while they also offer a better physical insight. The method described belongs to the class of integral transform methods. These are characterized by three basic ingredients: transformation with respect to the time coordinate plus the horizontal spatial coordinates, solution of the transform-domain differential equations, and inverse transformation back to the space–time domain. For each of these basic operations various techniques exist. In general, these techniques cannot be chosen independently of each other, and a specific combination determines the capabilities of the resulting method, no method being ideal in every respect.

For a long time integral transform methods have been applied to configurations with piecewise homogeneous layers (Spencer 1960; Helmberger 1968; Müller 1970). As a step towards a continuously layered configuration, models with fine homogeneous layers have been introduced (Wiggins & Helmberger 1974). Finally, integral transform methods are applied to investigate wave propagation in purely continuously layered configurations. It is possible to start with a finely layered model and subsequently perform a limiting procedure to arrive at the continuous situation (Bremmer 1939, 1951; Chapman 1974a), or use an approach in which the continuous behaviour of the medium parameters is understood directly (Chapman 1974a, 1976; Kennett & Illingworth 1981; Kennett 1983).

As far as the time coordinate is concerned, the Fourier or Laplace transformation is commonly used. In the literature one most often encounters the frequency-domain approach, which implies the application of the Fourier transformation with a real transformation parameter ω, the angular frequency. The Laplace transformation with real and positive transformation

parameter is less frequently employed, but takes causality explicitly into account. In the vast majority of cases some version of the Fourier transformation is used for the spatial transformation with respect to the horizontal coordinates (Morse & Feshbach 1953; Chapman 1978; Aki & Richards 1980; Ben Menahem & Singh 1981; Kennett 1983).

To solve the transform-domain differential equation there are, irrespective of the detailed versions of the transformations, four important methods: the WKBJ and Langer asymptotic expansions, and the WKBJ and Langer iterative solutions (Chapman 1981; Kennett 1983; Chapman & Orcutt 1985). The terms of the asymptotic expansions are simple, but reflected waves are poorly recognized in them. The iterative methods give a comprehensible expansion in terms of reflected wave components, but the iteration steps can become quite elaborate. The advantage of both WKBJ methods is that they represent the wave propagation in terms of exponential functions. They can be regarded as an extension of the well-known (first order) WKBJ asymptotic approximation. A common difficulty of WKBJ methods is that they break down if somehow the vertical propagation coefficient becomes zero (e.g., at a turning point in the frequency-domain approach). The Langer methods use Airy functions that handle the latter difficulty. They have been designed to possess a uniform validity (Langer 1937; Wasow 1965) and their use in seismology is widespread (Chapman 1974b; Kennett & Illingworth 1981; Garmany 1988b). There is still another technique to avoid difficulties with a zero value propagation coefficient. It uses a simple local asymptotic expansion in terms of Airy functions to determine the 'reflection factor' of a turning point, which can subsequently be implemented in WKBJ methods at places where these used to fail (Budden 1961; Garmany 1988a). It is observed that traditionally the notion 'WKBJ' has been used only in connection with the frequency domain, but in the present literature it is used in a broader sense.

The final operation is the transformation back to the space–time domain, which is performed using the corresponding inverse integral transformations. If we have used a Fourier transformation with a real angular frequency with respect to time, the original paths of integration of the inverse spatial Fourier transformation run through points where the propagation coefficient becomes zero, while with the Laplace transformation with a real and positive transformation parameter this difficulty does not show up. Irrespective of the specific versions of inverse temporal and spatial transformations, several methods have been derived to avoid a direct numerical evaluation of the inversion integrals. The spectral method, either with a real contour of integration as in the reflectivity method, or with a complex countour of integration as in the 'full wave theory' (Choy 1977), yields two important ways of achieving this. Two other possibilities are formed by the slowness method with either a real contour of integration, often called the Chapman method (Chapman 1978), or with a complex contour of integration, which is known as the modified Cagniard method, the Cagniard–De Hoop method or the generalized ray method (Cagniard 1939; De Hoop 1960, 1961, 1988; Pao & Gajewski 1977). An outline of these four important methods can be found in Chapman (1978) and Chapman & Orcutt (1985).

Based upon the ingredients discussed so far, a multitude of combinations can be used to solve the problem. To select out of these the most appropriate one, the following criteria are taken: the method should be generally applicable, exact, mathematically straightforward and physically instructive.

To avoid the difficulties associated with a propagation coefficient that becomes zero during the inverse spatial transformation, it seems logical to select the Laplace transformation with a real and positive transformation parameter with respect to time, rather than the Fourier transformation with a real angular frequency. On the basis of generality, the transform-domain differential equation should be solved by a preferably convergent, iterative scheme instead of any asymptotic expansion (the latter usually break down if the parameter profile has some discontinuous derivative). Regarding the transformation back to the space–time domain we are in favour of the slowness methods, which allow for an analytic evaluation of the inverse transformation with respect to time, as opposed to the spectral methods, for which all inverse transformations must in general be evaluated numerically.

As far as the iterative techniques for solving the transform-domain differential equations are concerned, we prefer the WKBJ iterative solution, in which now no breakdown occurs on the original paths of integration, over the Langer iterative solution, which in our case is unnecessarily intricate. In the process of contour deformation as a part of the inverse transformation, we do meet under some circumstances points in the complex slowness plane where the propagation coefficient becomes zero. However, from the application of Cauchy's theorem we know how to encircle such a point (if it occurs) and how to take into account its contribution. Also, zeroes of an arbitrarily high order can be treated. For the latter the Langer iterative solution breaks down and one has to take recourse to the solutions of differential equations with higher order zeroes in their coefficients (Chapman 1981, section 6).

As a result, we are only left with two possibilities: a combination of the WKBJ iterative solution with the modified Cagniard method or a combination of the WKBJ iterative solution with the Chapman method. Unfortunately, most of the elegance of the Chapman method is lost if it is used to perform an exact inversion, while the more attractive approximate version only yields correct answers near the arrival time of the wavefronts. Although the combination of the WKBJ iterative solution and the Chapman method is often used, it does not quite satisfy our requirements.

Finally, upon combining the WKBJ iterative solution with the modified Cagniard method, we obtain a method that is completely suited to our purpose. Although this combination has been applied before (Chapman 1974a, 1976), in our opinion some questions have remained up till now. The major point concerns the extension of the method to cope with all kinds of continuously layered configurations, not only the ones with parameter profiles that strictly increase with depth. Another

question remains about the convergence of the iterative solution. This convergence has been proved for the geometrical approximation near the arrival time (Chapman 1976), but general convergence statements are rare. Finally, we mention the problem of how the various shapes of the modified Cagniard contours are related to the parameter profiles of a given configuration and what ray shapes are associated with them. All these aspects will be covered in our analysis.

2 CONFIGURATION AND BASIC EQUATIONS

The configuration to be investigated is shown in Fig. 1. It consists of a point-source that starts to act at the instant $t = 0$, and a receiver, amenable to measure the wavefield quantities. Both are situated in a medium that extends to infinity in all directions. The medium is invariant in the horizontal directions x_1 and x_2, while its properties may vary in *any* continuous fashion in the vertical direction x_3. The implicit or explicit restriction that the wavespeed profile should be a monotonic function of depth, which has been often imposed in the literature (Chapman 1974a, 1976), is not imposed here. Further, the medium is linear, locally and instantaneously reacting, isotropic and time invariant.

To concentrate on the essentials of our approach, we restrict ourselves in this paper to acoustic wave propagation. Examples in which we encounter this kind of propagation are waves in fluids (e.g., waves in seawater) and the compressional waves in the equivalent fluid model of the Earth.

Using the subscript notation and the summation convention, where lower-case Latin subscripts range from 1 to 3, the space–time domain linearized acoustic equations can be written as

$$\partial_k v_k(x_i, t) + \kappa(x_3)\, \partial_t p(x_i, t) = q(x_i, t), \tag{1}$$

$$\partial_k p(x_i, t) + \rho(x_3)\, \partial_t v_k(x_i, t) = f_k(x_i, t). \tag{2}$$

Here, p is the acoustic pressure, v_k indicates the particle velocity, $\rho(x_3)$ is the volume density of mass of the medium, while $\kappa(x_3)$ is its compressibility. Further, ∂_t and ∂_k denote differentiation with respect to time and the coordinate x_k, respectively. The action of the source is accounted for by f_k, its volume density of volume force, and q, its volume density of volume injection rate. Throughout our investigation the source is taken to be a point-source, and without loss of generality we may assume that it is located on the vertical line through the origin of the chosen reference frame, so it can be represented by

$$\{q(x_i, t), f_k(x_i, t)\} = \{Q_k^S(t), F^S(t)\}\, \delta(x_1, x_2, x_3 - x_3^S). \tag{3}$$

Although in this paper we only treat the acoustical case, our approach can also be used for more complex kinds of wave propagation. As an example, in Appendix C we show how our approach can be applied in case of elastic media.

3 TRANSFORMATION OF THE BASIC EQUATIONS

We exploit the time invariance and the horizontal shift invariance of the configuration by applying appropriate integral transformations to the space–time domain basic equations. First we carry out a (one-sided) Laplace transformation with respect to time. As an example, the space–time domain quantity $p(x_i, t)$ is transformed to the space-temporal Laplace domain quantity $\hat{p}(x_i, s)$ according to

$$\hat{p}(x_i, s) = \int_{0^-}^{\infty} p(x_i, t) \exp(-st)\, dt. \tag{4}$$

Following Cagniard (1939), the transformation parameter s is taken real and positive. This choice is characteristic for the modified Cagniard method which we will employ to carry out the inverse transformation. The reason for using the Laplace transformation, with real s, instead of the more commonly used Fourier transformation with a real angular frequency ω is

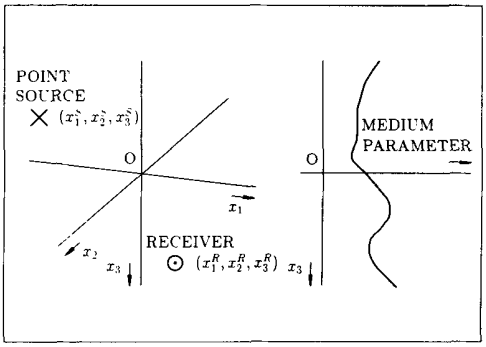

Figure 1. General continuously layered configuration.

two-fold: our choice results into a more convenient location of the branch points in the complex slowness plane that will be used in the modified Cagniard method, while causality in the space–time domain is ensured if in the space-temporal Laplace domain the quantities are regular for $s > s_0$, with s_0 a certain, positive value [Lerch's theorem; Widder (1946)]. Moreover, taking the Laplace transformation with a real variable s makes it possible to prove the convergence of the WKBJ iterative solution, both in the transform domain and, in view of Lerch's theorem, also in the time domain (De Hoop 1990).

Second, a 2-D spatial Fourier transformation with respect to x_1 and x_2 is carried out. The spatial Fourier–temporal Laplace domain counterpart or, shortly, the transform-domain counterpart $\hat{p}(\alpha_1, \alpha_2, x_3, s)$ of $\hat{p}(x_1, x_2, x_3, s)$ is defined by

$$\hat{p}(\alpha_1, \alpha_2, x_3, s) = \int_{-\infty}^{\infty} \int_{-\infty}^{\infty} \hat{p}(x_i, s) \exp\left[is(\alpha_1 x_1 + \alpha_2 x_2)\right] dx_1\, dx_2. \tag{5}$$

The corresponding inverse Fourier transformation is

$$\hat{p}(x_i, s) = \left(\frac{s}{2\pi}\right)^2 \int_{-\infty}^{\infty} \int_{-\infty}^{\infty} \hat{p}(\alpha_1, \alpha_2, x_3, s) \exp\left[-is(\alpha_1 x_1 + \alpha_2 x_2)\right] d\alpha_1\, d\alpha_2. \tag{6}$$

Note that the actual Fourier transformation parameters are $s\alpha_1$ and $s\alpha_2$. Here, too, the Laplace transformation with respect to time turns out to be more convenient than the Fourier transformation, since s is only positive, while ω can be both positive and negative, the latter case yielding additional difficulties in the inverse spatial Fourier transformation. For example, in Heyman & Felsen (1984) and Chapman (1978) we observe space-temporal Fourier expressions that contain $i\,\mathrm{sgn}(\omega)$, which correspond to a Hilbert transformation in the space–time domain.

Using the rotational symmetry of the configuration, we could also have chosen a Fourier series expansion with respect to the azimuthal angle in combination with a Hankel transformation with respect to the radial variable (see Achenbach 1973). As the Fourier series contains often only a few terms, we only have at inversion to evaluate a few inverse Hankel transformation integrals. This seems to be more efficient than evaluating equation (6). But later it will become clear that, if we apply the Cagniard–De Hoop method, we often get more trouble with a single inverse Hankel transformation than with a double inverse Fourier transformation.

Applying the respective transformations to the basic acoustic equations (1) and (2), eliminating $\hat{v}_1$ and $\hat{v}_2$ and using matrix notation, we arrive at the transform domain differential equation

$$\partial_3 \begin{pmatrix} \hat{v}_3 \\ \hat{p} \end{pmatrix} + s \begin{pmatrix} 0 & \gamma(x_3)Y(x_3) \\ \gamma(x_3)Y^{-1}(x_3) & 0 \end{pmatrix} \begin{pmatrix} \hat{v}_3 \\ \hat{p} \end{pmatrix} = \delta(x_3 - x_3^{\mathrm{S}}) \begin{pmatrix} \hat{\hat{Q}}^{\mathrm{S}} \\ \hat{\hat{F}}^{\mathrm{S}} \end{pmatrix}, \tag{7}$$

in which

$$\gamma(x_3) = [c^{-2}(x_3) + \alpha_1^2 + \alpha_2^2]^{1/2} \tag{8}$$

is the vertical propagation coefficient or vertical slowness,

$$Y(x_3) = \frac{\gamma(x_3)}{\rho(x_3)} \tag{9}$$

is the vertical acoustic wave admittance, and

$$\begin{pmatrix} \hat{\hat{Q}}^{\mathrm{S}} \\ \hat{\hat{F}}^{\mathrm{S}} \end{pmatrix} = \begin{pmatrix} \hat{Q}^{\mathrm{S}}(s) + \rho^{-1}(x_3)[i\alpha_1 \hat{F}_1^{\mathrm{S}}(s) + i\alpha_2 \hat{F}_2^{\mathrm{S}}(s)] \\ \hat{F}_3^{\mathrm{S}}(s) \end{pmatrix} \tag{10}$$

is the transform-domain notional source strength vector. In equation (8)

$$c(x_3) = [\rho(x_3)\kappa(x_3)]^{-1/2} \tag{11}$$

is the acoustic wavespeed. Note that with our transformation scheme, $\gamma(x_3)$ and $Y(x_3)$ are real and positive. Using subscript notation and the summation convention once more, where upper case Latin subscripts are assigned the values 1 and 2, we can rewrite (7) as

$$\partial_3 \hat{\hat{\mathbf{b}}}_I + s\mathbf{A}_{IJ}(x_3)\hat{\hat{\mathbf{b}}}_J = \hat{\hat{\mathbf{u}}}_I. \tag{12}$$

In this equation $\hat{\hat{\mathbf{b}}}_I$ is denoted as the acoustic state vector, $\mathbf{A}_{IJ}(x_3)$ is the system matrix and $\hat{\hat{\mathbf{u}}}_I$ is the source strength vector.

4 SOLUTION OF THE RESULTING SYSTEM OF FIRST-ORDER DIFFERENTIAL EQUATIONS

There are many ways in which we can find an exact or approximate solution of the transform domain equation (12). A clear outline of these methods has been given by Chapman (1981), Chapman & Orcutt (1985) and Kennett (1983) for the case where a Fourier transformation with respect to time has been used. There are two reasons for showing our own method of finding an

exact solution: first of all, the fact that we have used the Laplace transformation with respect to time has some important consequences for the existence and uniqueness of the solution; second, our method differs from those commonly used in the literature, as we do not solve the differential equation using the reduced wave vector (from which the exponential behaviour has been removed), but use Green's functions and the superposition principle to find the solution of the wave vector differential equation.

As a first step, following the literature (Chapman 1974a, 1976; Kennett 1983), we decompose the system matrix $\mathbf{A}_{IJ}(x_3)$ into

$$\mathbf{A}_{IJ}(x_3) = \mathbf{N}_{IK}(x_3)\mathbf{\Lambda}_{KL}(x_3)\mathbf{N}^{-1}_{LJ}(x_3). \tag{13}$$

In this equation

$$\mathbf{\Lambda}_{KL}(x_3) = \begin{pmatrix} \gamma(x_3) & 0 \\ 0 & -\gamma(x_3) \end{pmatrix}, \tag{14}$$

is the eigenvalue matrix of $\mathbf{A}_{IJ}(x_3)$, whereas

$$\mathbf{N}_{IK}(x_3) = \tfrac{1}{2}\sqrt{2}\begin{pmatrix} Y^{1/2}(x_3) & -Y^{1/2}(x_3) \\ Y^{-1/2}(x_3) & Y^{-1/2}(x_3) \end{pmatrix}, \tag{15}$$

is the composition matrix and

$$\mathbf{N}^{-1}_{LJ}(x_3) = \tfrac{1}{2}\sqrt{2}\begin{pmatrix} Y^{-1/2}(x_3) & Y^{1/2}(x_3) \\ -Y^{-1/2}(x_3) & Y^{1/2}(x_3) \end{pmatrix}. \tag{16}$$

is the decomposition matrix. At this point, we define the wave vector $\hat{\tilde{\mathbf{w}}}_J$ through the composition relation

$$\hat{\tilde{\mathbf{b}}}_I = \mathbf{N}_{IJ}(x_3)\hat{\tilde{\mathbf{w}}}_J. \tag{17}$$

Using equations (12) and (17), the wave vector differential equation is found as

$$\partial_3\hat{\tilde{\mathbf{w}}}_I + s\mathbf{\Lambda}_{IJ}(x_3)\hat{\tilde{\mathbf{w}}}_J = \mathbf{\Delta}(x_3)_{IK}\hat{\tilde{\mathbf{w}}}_K + \mathbf{N}^{-1}_{IJ}(x_3)\hat{\tilde{\mathbf{u}}}_J. \tag{18}$$

The so-called coupling matrix $\mathbf{\Delta}_{IK}(x_3)$ is given by

$$\mathbf{\Delta}_{IK}(x_3) = -\mathbf{N}^{-1}_{IJ}(x_3)[\partial_3\mathbf{N}(x_3)]_{JK} = \begin{pmatrix} 0 & \chi(x_3) \\ \chi(x_3) & 0 \end{pmatrix}, \tag{19}$$

in which $\chi(x_3) = \partial_3 Y(x_3)/2Y(x_3) = \frac{1}{2}\partial_3[\ln Y(x_3)]$ is the inhomogeneity function. Equations (17)–(19) are equivalent to (55)–(57) in Chapman (1974a). The source part of (18) becomes

$$\mathbf{N}^{-1}_{IJ}(x_3)\hat{\tilde{\mathbf{u}}}_J = \tfrac{1}{2}\sqrt{2}\,\delta(x_3 - x_3^{\mathrm{S}})\begin{pmatrix} A \\ B \end{pmatrix}, \tag{20}$$

with

$$A = \hat{\tilde{F}}^{\mathrm{S}}Y^{1/2}(x_3^{\mathrm{S}}) + \hat{\tilde{Q}}^{\mathrm{S}}Y^{-1/2}(x_3^{\mathrm{S}}), \tag{21}$$

$$B = \hat{\tilde{F}}^{\mathrm{S}}Y^{1/2}(x_3^{\mathrm{S}}) - \hat{\tilde{Q}}^{\mathrm{S}}Y^{-1/2}(x_3^{\mathrm{S}}). \tag{22}$$

Next, we determine the causal Green's functions of the left-hand side of (18) that satisfy

$$\partial_3\hat{\tilde{g}}_1 + s\gamma(x_3)\hat{\tilde{g}}_1 = \delta(x_3 - x_3'), \tag{23}$$

$$\partial_3\hat{\tilde{g}}_2 - s\gamma(x_3)\hat{\tilde{g}}_2 = \delta(x_3 - x_3'). \tag{24}$$

They are found as

$$\hat{\tilde{g}}_1(x_3, x_3') = H(x_3 - x_3')\exp\left(-s\int_{x_3'}^{x_3}\gamma\,d\zeta\right), \tag{25}$$

$$\hat{\tilde{g}}_2(x_3, x_3') = -H(x_3' - x_3)\exp\left(-s\int_{x_3}^{x_3'}\gamma\,d\zeta\right). \tag{26}$$

In equations (25) and (26), H denotes the Heaviside unit step function. Knowing $\hat{\tilde{g}}_1$ and $\hat{\tilde{g}}_2$, we can apply a superposition integral with respect to the vertical coordinate and obtain

$$\hat{\tilde{w}}_1(x_3) = \int_{-\infty}^{\infty}\chi(x_3')\hat{\tilde{g}}_1(x_3, x_3')\hat{\tilde{w}}_2(x_3')\,dx_3' + \tfrac{1}{2}\sqrt{2}\,A\hat{\tilde{g}}_1(x_3, x_3^{\mathrm{S}}), \tag{27}$$

$$\hat{\tilde{w}}_2(x_3) = \int_{-\infty}^{\infty}\chi(x_3')\hat{\tilde{g}}_2(x_3, x_3')\hat{\tilde{w}}_1(x_3')\,dx_3' + \tfrac{1}{2}\sqrt{2}\,B\hat{\tilde{g}}_2(x_3, x_3^{\mathrm{S}}). \tag{28}$$

We solve this system by using a straightforward vectorial extension of the theory of scalar integral equations. To this end we rewrite (27) and (28) as an operator equation

$$\hat{\tilde{\mathbf{w}}}_I = \mathbf{L}_{IJ}\hat{\tilde{\mathbf{w}}}_J + \hat{\tilde{\mathbf{h}}}_I, \tag{29}$$

in which the integral operator $\mathbf{L}_{IJ}$ is defined by

$$\mathbf{L}_{IJ}\hat{\tilde{\mathbf{w}}}_J = \begin{pmatrix} \displaystyle\int_{-\infty}^{x_3} \chi(x_3') \exp\left(-s\int_{x_3'}^{x_3} \gamma\, d\zeta\right)\hat{\tilde{w}}_2\, dx_3' \\ \displaystyle -\int_{x_3}^{\infty} \chi(x_3') \exp\left(-s\int_{x_3}^{x_3'} \gamma\, d\zeta\right)\hat{\tilde{w}}_1\, dx_3' \end{pmatrix}, \tag{30}$$

where the integration limits follow from the step functions in (25) and (26). The source vector $\hat{\tilde{\mathbf{h}}}_I$ is

$$\hat{\tilde{\mathbf{h}}}_I = \begin{pmatrix} \frac{1}{2}\sqrt{2}\, AH(x_3 - x_3^{\mathrm{S}}) \exp\left(-s\displaystyle\int_{x_3^{\mathrm{S}}}^{x_3} \gamma\, d\zeta\right) \\ -\frac{1}{2}\sqrt{2}\, BH(x_3^{\mathrm{S}} - x_3) \exp\left(-s\displaystyle\int_{x_3}^{x_3^{\mathrm{S}}} \gamma\, d\zeta\right) \end{pmatrix}. \tag{31}$$

Upon rewriting equation (29) as

$$\hat{\tilde{\mathbf{w}}}_I = (\mathbf{I} - \mathbf{L})_{IJ}^{-1}\hat{\tilde{\mathbf{h}}}_J, \tag{32}$$

and application of the Neumann series for the operator $(\mathbf{I} - \mathbf{L})_{IJ}^{-1}$, we arrive at

$$\hat{\tilde{\mathbf{w}}}_I = (\mathbf{I}_{IJ} + \mathbf{L}_{IJ} + \mathbf{L}_{IJ}^2 + \cdots)\hat{\tilde{\mathbf{h}}}_J. \tag{33}$$

This is of the form

$$\hat{\tilde{\mathbf{w}}}_I = \hat{\tilde{\mathbf{w}}}_I^{(0)} + \hat{\tilde{\mathbf{w}}}_I^{(1)} + \hat{\tilde{\mathbf{w}}}_I^{(2)} + \cdots, \tag{34}$$

in which

$$\hat{\tilde{\mathbf{w}}}_I^{(i)} = \begin{cases} \hat{\tilde{\mathbf{h}}}_I & (i = 0), \\ (\mathbf{L}^i)_{IJ}\hat{\tilde{\mathbf{h}}}_J = \mathbf{L}_{IJ}\hat{\tilde{\mathbf{w}}}_J^{(i-1)} & (i = 1, 2, \ldots). \end{cases} \tag{35}$$

Using (30) and (31), equation (35) leads to

$$\hat{\tilde{w}}_1^{(0)} = \tfrac{1}{2}\sqrt{2}\, AH(x_3 - x_3^{\mathrm{S}}) \exp\left(-s\int_{x_3^{\mathrm{S}}}^{x_3} \gamma\, d\zeta\right), \tag{36}$$

$$\hat{\tilde{w}}_2^{(0)} = -\tfrac{1}{2}\sqrt{2}\, BH(x_3^{\mathrm{S}} - x_3) \exp\left(-s\int_{x_3}^{x_3^{\mathrm{S}}} \gamma\, d\zeta\right), \tag{37}$$

and

$$\hat{\tilde{w}}_1^{(i)} = \int_{-\infty}^{x_3} \chi(x_3') \exp\left(-s\int_{x_3'}^{x_3} \gamma\, d\zeta\right)\hat{\tilde{w}}_2^{(i-1)}\, dx_3' \qquad (i = 1, 2, \ldots), \tag{38}$$

$$\hat{\tilde{w}}_2^{(i)} = -\int_{x_3}^{\infty} \chi(x_3') \exp\left(-s\int_{x_3}^{x_3'} \gamma\, d\zeta\right)\hat{\tilde{w}}_1^{(i-1)}\, dx_3' \qquad (i = 1, 2, \ldots). \tag{39}$$

The convergence of the series has been treated extensively by De Hoop (1990). In view of the fact that the Laplace transformation parameter s is real and can be chosen arbitrarily large, the elements of the operator $\mathbf{L}_{IJ}$ in equation (30) can be made arbitrarily small, provided that $\gamma(x_3)$ is always non-zero and that $\chi(x_3)$ remains bounded.

For all real values of α_1 and α_2, i.e., those values used in connection with the inverse spatial Fourier transformation, the first requirement will always be met, while the second requirement is met for *every* configuration with continuous parameter profiles. This means that the transform-domain Neumann series solution is convergent under *all* circumstances, for *any* continuously layered configuration. Moreover, Lerch's theorem (Widder 1946) states that the convergence carries over to the causal time-domain solution. At this point it should be noted that application of the Fourier transformation with respect to time would yield an equivalent series solution, the well-known WKBJ iterative solution (Chapman 1981). However, due to the fact that s is then replaced by $i\omega$, which becomes zero during the inversion process, the convergence can be proved for a *restricted* class of continuously layered configurations only, and the causality is not guaranteed automatically since a Fourier equivalent of Lerch's theorem does not exist. To be compatible with the frequency-domain terminology, we will from now on use the notion WKBJ iterative solution instead of Neumann series solution, although a Laplace transformation with respect to time has been applied.

Once we know the series solution of the wave vector $\hat{\mathbf{w}}_I$, we can apply the composition relation (17) to obtain the series solution of the acoustic state vector $\hat{\mathbf{b}}_I$. The explicit expressions for the zeroth-order term of $\hat{\mathbf{b}}_I$ at the position (x_i^R) of the receiver are

$$\hat{\mathbf{b}}_I^{(0)} = \tfrac{1}{2}A \exp\left(-s\int_{x_3^S}^{x_3^R} \gamma\, d\zeta\right)\begin{pmatrix} Y^{1/2}(x_3^R) \\ Y^{-1/2}(x_3^R)\end{pmatrix} \qquad (x_3^R > x_3^S), \tag{40}$$

$$\hat{\mathbf{b}}_I^{(0)} = \tfrac{1}{2}B \exp\left(-s\int_{x_3^R}^{x_3^S} \gamma\, d\zeta\right)\begin{pmatrix} -Y^{1/2}(x_3^R) \\ Y^{-1/2}(x_3^R)\end{pmatrix} \qquad (x_3^R < x_3^S). \tag{41}$$

The first-order term of $\hat{\mathbf{b}}_I$ at the receiver is given by

$$\hat{\mathbf{b}}_I^{(1)} = -\tfrac{1}{2}B\int_{-\infty}^{m} \chi(x_3) \exp\left[-s\left(\int_{x_3}^{x_3^S} \gamma\, d\zeta + \int_{x_3}^{x_3^R} \gamma\, d\zeta\right)\right] dx_3 \begin{pmatrix} Y^{1/2}(x_3^R) \\ Y^{-1/2}(x_3^R)\end{pmatrix} +$$
$$-\tfrac{1}{2}A\int_{M}^{\infty} \chi(x_3) \exp\left[-s\left(\int_{x_3^S}^{x_3} \gamma\, d\zeta + \int_{x_3^R}^{x_3} \gamma\, d\zeta\right)\right] dx_3 \begin{pmatrix} -Y^{1/2}(x_3^R) \\ Y^{-1/2}(x_3^R)\end{pmatrix}, \tag{42}$$

in which

$$m = \min\{x_3^R, x_3^S\}, \tag{43}$$

$$M = \max\{x_3^R, x_3^S\}, \tag{44}$$

indicate the various situations that can occur with regard to relative vetical positions x_3^R of the point of observation and x_3^S of the source. In the next section we shall explain the physical interpretation of the terms in the WKBJ iterative solution in general and of the zeroth- and first-order terms in particular. In Sections 6 and 7 we shall perform the transformation back to the space–time domain of the zeroth- and first-order terms, respectively.

5 PHYSICAL INTERPRETATION

The results of equations (36)–(39) indicate that $\hat{w}_1^{(0)}, \hat{w}_1^{(1)}, \ldots$, represent waves that travel in the direction of increasing x_3, while $\hat{w}_2^{(0)}, \hat{w}_2^{(1)}, \ldots$, represent waves that travel in the direction of decreasing x_3.

The direct or zeroth-order waves $\hat{w}_1^{(0)}$ and $\hat{w}_2^{(0)}$ are directly generated by the source. This is reflected by the fact that

$$\lim_{x_3 \downarrow x_3^S} \hat{\mathbf{w}}_I^{(i)} = \lim_{x_3 \uparrow x_3^S} \hat{\mathbf{w}}_I^{(i)} \qquad (i = 1, 2, \ldots), \tag{45}$$

i.e., $\hat{w}_1^{(i)}$ and $\hat{w}_2^{(i)}$ $(i = 1, 2, \ldots)$ are continuous upon crossing the source level. In Fig. 2 the propagation of $\hat{w}_1^{(0)}$ and $\hat{w}_2^{(0)}$ is shown; these wave vector components only exist for $x_3^R > x_3^S$ and $x_3^R < x_3^S$, respectively. The expressions for the corresponding zeroth-order acoustic state vectors are given in equations (40) and (41).

Next, a zeroth-order wave generates, by continuous reflection against the inhomogeneous medium, a secondary or first-order wave, travelling in the opposite direction. Equations (38) and (39) are a mathematical formulation of ths process: $\hat{w}_1^{(0)}$ generates $\hat{w}_2^{(1)}$ and $\hat{w}_2^{(0)}$ generates $\hat{w}_1^{(1)}$ (incident waves generating reflected waves that travel in the opposite direction), depending upon $\chi(x_3)$ (representing the degree of inhomogeneity of the medium), by means of an integration with respect to the vertical coordinate (continuous summation of the partial reflections).

In Fig. 3 we illustrate the generation of the first-order waves according to this process. Different situations can occur, depending upon the relative vertical positions of the source x_3^S and the points of observations x_3^R. We take $\hat{w}_2^{(1)}$ as an example.

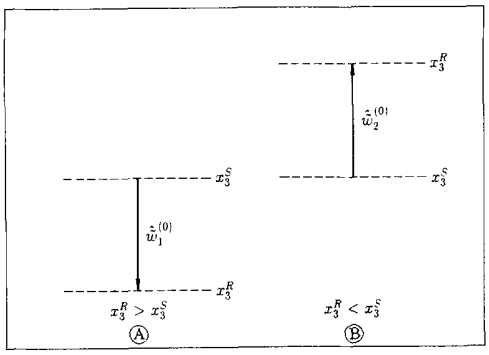

Figure 2. Propagation of zeroth-order wave vector components; (a) propagation in the direction of increasing x_3; (b) propagation in the direction of decreasing x_3.

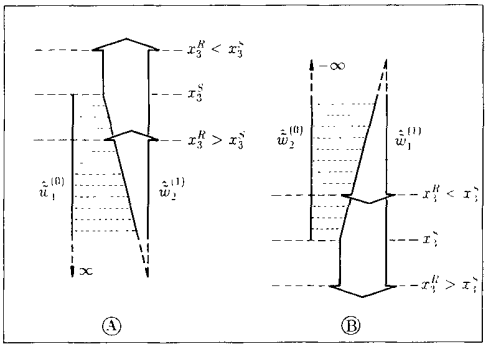

Figure 3. Generation of the first-order wave vector components; (a) components travelling in the direction of decreasing x_3; (b) components travelling in the direction of increasing x_3.

Using (37) and (38), we obtain two different expressions for $\hat{\tilde{w}}_2^{(1)}$, depending on the integration limit M; they are

$$\hat{\tilde{w}}_2^{(1)} = -\tfrac{1}{2}\sqrt{2}\,A\int_{x_3^R}^{\infty}\chi(x_3)\exp\left[-s\left(\int_{x_3^R}^{x_3}\gamma\,d\zeta+\int_{x_3^S}^{x_3}\gamma\,d\zeta\right)\right]dx_3 \qquad (x_3^R>x_3^S), \tag{46}$$

$$\hat{\tilde{w}}_2^{(1)} = -\tfrac{1}{2}\sqrt{2}\,A\int_{x_3^S}^{\infty}\chi(x_3)\exp\left[-s\left(\int_{x_3^S}^{x_3}\gamma\,d\zeta+\int_{x_3^R}^{x_3}\gamma\,d\zeta\right)\right]dx_3 \qquad (x_3^R<x_3^S). \tag{47}$$

If equation (46) holds, the entire interval $[x_3^R;\infty\rangle$ yields contributions to $\hat{\tilde{w}}_2^{(1)}(x_3^R)$, unless $\chi(x_3)=0$, since $\hat{\tilde{w}}_1^{(0)}$ is non-zero at all $x_3^R>x_3^S$. However, if (47) is to be used, only the interval $[x_3^S;\infty\rangle$ contributes to $\hat{\tilde{w}}_2^{(1)}(x_3^R)$, as for $x_3^R<x_3^S$ the direct wave $\hat{\tilde{w}}_1^{(0)}$ is zero on $[x_3^R;x_3^S]$, yielding no contributions to $\hat{\tilde{w}}_2^{(1)}$. Both situations are depicted in Fig. 3(a).

The process of continuous reflection also results in higher order waves. Generally, a wave of order $(n-1)$ generates a nth-order wave travelling in the opposite direction. This is incorporated in equations (38) and (39) as well.

The above process can also be described in terms of generalized rays (Spencer 1960; Helmberger 1968; Wiggins & Helmberger 1974). Using this concept, we can state that the zeroth-order wave arriving at x_3^R is represented by a single ray from x_3^S to x_3^R, in accordance with equation (36) or (37). The generation of the first-order waves by continuous reflection of a zeroth-order wave is represented by rays that originate at x_3^S, reflect at x_3 and finally arrive at x_3^R. Now an infinite number of such reflecting rays has to be superimposed to give the complete first-order result. This process has been described by equations (38) and (39) with $i=1$. In an equivalent manner, kth-order waves are represented by a repeated, continuous summation of rays that originate at x_3^S, are reflected at $x_3, x_3', \ldots, x_3^{(k)}$, and finally arive at x_3^R.

6 TRANSFORMATION BACK TO THE SPACE–TIME DOMAIN: ZEROTH-ORDER COMPONENTS

After the transform domain acoustic state vector has been found, we must apply the inverse transformations to return to the space–time domain. Compared with the forward transformations (4) and (5), the inverse transformations are not so easy to perform. Although they can be evaluated purely numerically, our specific configuration allows for more efficient methods. In our approach we apply the modified Cagniard method of inversion (De Hoop 1960, 1961, 1988; Pao & Gajewski 1977; Van der Hijden 1987). Chapman (1974a, 1976) also combines the WKBJ iterative solution and the modified Cagniard method, but our derivations differ considerably, mainly because continuous parameter profiles of a general shape are assumed.

It is observed that the application of the Laplace transformation with respect to time already ensures the convergence of the WKBJ iterative solution, both in the transform domain as well as in the space–time domain. In view of Cauchy's theorem, the inverse transformation process for each term of this series solution may contain a deformation of the path of integration, without changing the space–time domain results for each term, provided that singularities are treated correctly. The fact that with the modified Cagniard method we have to take care of points where $\gamma(x_3)=0$ is purely imposed to obtain a correct contour deformation but plays no part in the validity of the WKBJ iterative solution. This means that difficulties with some other methods, such as those caused by turning rays etc., do not show up in our approach.

The goal of this section is to illustrate the inverse transformation method for the zeroth-order components. To avoid repetition of similar equations for all those components, we confine ourselves in this section to a zeroth-order pressure wave travelling upwards from a source, representing some subsurface event, to a receiver located on a more elevated level. The configuration is shown in Fig. 4. The pressure wave will be indicated by $p^{(0)-}$, where the superscript $^{(0)}$ indicates the order and the minus sign refers to the direction of propagation.

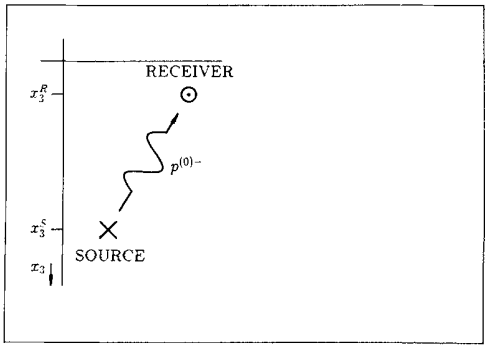

Figure 4. Configuration in which the zeroth-order pressure wave propagates.

6.1 Introduction of zeroth-order Green's functions

Upon applying the inverse Fourier transformation (6) to equation (41), we obtain an expression for $\hat{p}^{(0)-}$, which can formally be written as

$$\hat{p}^{(0)-} = s^2\hat{F}_1^S(s)\hat{G}_{f_1}^{(0)-} + s^2\hat{F}_2^S(s)\hat{G}_{f_2}^{(0)-} + s^2\hat{F}_3^S(s)\hat{G}_{f_3}^{(0)-} + s^2\hat{Q}^S(s)\hat{G}_q^{(0)-}. \tag{48}$$

The benefit of this representation is that the Green's functions $\hat{G}^{(0)-}$ are independent of the signatures of the associated sources. As the inversion procedure is the same for each zeroth-order Green's function, we assume for brevity that the source is of the volume injection type, and we only consider

$$\hat{G}_q^{(0)-} = \frac{-1}{8\pi^2}\int_{-\infty}^{\infty}\int_{-\infty}^{\infty}\Pi\exp\left[-s\left(i\alpha_1 x_1 + i\alpha_2 x_2 + \int_{x_3^R}^{x_3^S}\gamma\, d\zeta\right)\right]d\alpha_1\, d\alpha_2, \tag{49}$$

where

$$\Pi = Y^{-1/2}(x_3^S)Y^{-1/2}(x_3^R). \tag{50}$$

6.2 Transformation of the variables α_1 and α_2 into p and q

In our case the inversion process involves a 2-D inverse Fourier transformation. With the Cagniard–De Hoop method it is then convenient to perform the transformation

$$\alpha_1 = -ip\cos\theta + q\sin\theta, \tag{51}$$

$$\alpha_2 = -ip\sin\theta - q\cos\theta, \tag{52}$$

where θ follows from the cylindrical coordinates of the receiver with respect to the source

$$r = \sqrt{(x_1^R)^2 + (x_2^R)^2}, \qquad \theta = \arctan\left(\frac{x_2^R}{x_1^R}\right), \qquad z = x_3^S - x_3^R. \tag{53}$$

The variable r is the horizontal offset of the receiver,while p is the horizontal slowness. To obtain the equivalent of equation (49) we must keep p imaginary and q real. It follows as

$$\hat{G}_q^{(0)-} = \frac{i}{8\pi^2}\int_{-\infty}^{\infty}\int_{-i\infty}^{i\infty}\bar{\Pi}\exp\left[-s\left(pr + \int_{x_3^R}^{x_3^S}\bar{\gamma}\, d\zeta\right)\right]dp\, dq. \tag{54}$$

Quantities in which α_1, α_2 are replaced by p, q are indicated by an overbar; the vertical propagation coefficient or vertical slowness is now given by

$$\bar{\gamma}(x_3) = [c^{-2}(x_3) - p^2 + q^2]^{1/2}. \tag{55}$$

Next we want to continue the integrand analytically into the complex p-plane. We define $\mathcal{R}e\,(\bar{\gamma}) \geq 0$ in order to keep the square root in equation (55) single valued. Also we must investigate the singularities of the integrand in (54). These are branch points due to $\bar{\gamma}(x_3^S)$ and $\bar{\gamma}(x_3^R)$ in the denominator and due to the integral of $\bar{\gamma}(\zeta)$ in the argument of the exponential function. The latter are $p^S = [c^{-2}(x_3^S) + q^2]^{1/2}$ and $p^R = [c^{-2}(x_3^R) + q^2]^{1/2}$ *and* the points $p^j = [c^{-2}(x_3^j) + q^2]^{1/2}$, with $x_3^R \leq x_3^j \leq x_3^S$ ($j = 1, \ldots, n$) forming the endpoints of the intervals where $\bar{\gamma}^j(\zeta) = [c^{-2}(\zeta) - (p^j)^2 + q^2]^{1/2}$ can be continued analytically into a complex ζ-plane. All branch points will be provided with branch cuts along the positive and negative real p-axis, respectively, from the relevant branch point to infinity. No other singularities are present. In Fig. 5 the singularities in the p-plane are depicted. Since we will apply Jordan's lemma, we are only allowed to deform our path of integration into the right half of the p-plane.

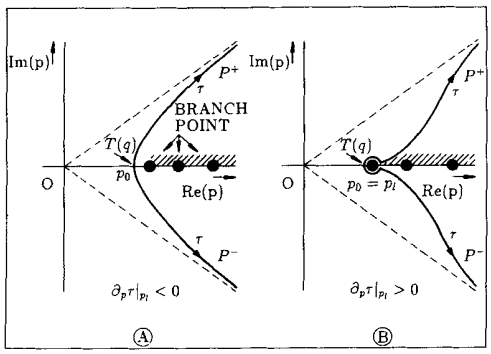

Figure 5. Possible locations of the modified Cagniard contour and the branch points in the right half of the complex p-plane. For case (b) the detour around the branch point has already been made.

6.3 The modified Cagniard path

Next we deform the path of integration from the imaginary p-axis into the so-called modified Cagniard path, defined by

$$\tau = pr + \int_{x_3^R}^{x_3^S} \bar{\gamma}(\zeta)\, d\zeta, \tag{56}$$

where p is such that τ is always real. The features of the modified Cagniard contours in continuously layered configurations have been summarized in Appendix A; they have not been discussed extensively in the literature [Chapman (1974a) forms one of the exceptions]. We note that in the continuously layered case, there are two possible types of contours, depending upon the sign of the quantity

$$\partial_p \tau|_{p_l} = r - p_l \int_{x_3^R}^{x_3^S} [c^{-2}(\zeta) - p_l^2 + q^2]^{-1/2}\, d\zeta, \tag{57}$$

where p_l is the leftmost branch point in the complex p-plane, i.e., $p_l = p_l(q) = (c_{\max}^{-2} + q^2)^{1/2}$ with $c_{\max} = \max_{\zeta \in [x_3^R; x_3^S]}\{c(\zeta)\}$. If $\partial_p \tau|_{p_l} < 0$, the countour crosses the real p-axis vetically in a point p_0 to the left of p_l, so there is no interference with the branch cuts. If $\partial_p \tau|_{p_l} > 0$, *a case which is impossible for piecewise homogeneous configurations*, the complex part of the countour meets the real axis horizonatally in $p_0 = p_l$. In Appendix B the relation between the shape of the modified Cagniard contour and the shape of the generalized ray associated with the point p_0, has been investigated. An important result is that if $\partial_p \tau|_{p_l} > 0$, this quantity is the length of the horizontal trajectory of a ray, whereas $\partial_p \tau|_{p_l} < 0$ means that the ray does not have any horizontal part. We note that the ray paths are located within the vertical interval $[x_3^R; x_3^S]$ only.

In the first and fourth quadrants we can form closed loops consisting of the positive or negative imaginary axis, a part of the positive real axis, the upper (P^+) or lower (P^-) branches of the contour and closing circular arcs at infinity. Applying Cauchy's theorem and Jordan's lemma to these loops, we find that the integration along the imaginary p-axis can be replaced by an integration along the complex part of the modified Cagniard contour. If $\partial_p \tau|_{p_l} < 0$, this can be done without any precautions, see Fig. 5(a). However, if $\partial_p \tau|_{p_l} > 0$ the modified Cagniard contour must be supplemented by a small circle with radius $\delta > 0$ in order to go around the leftmost branch point, see Fig. 5(b). In the limit $\delta \to 0$, this circle gives a vanishing contribution to the total integral. The contour is symmetrical with respect to the real p-axis and the integrand satisfies Schwarz' reflection principle; the integrand is also symmetrical with respect to q. Hence, we can rewrite (54) as

$$\hat{G}_q^{(0)-} = \frac{-1}{2\pi^2} \int_0^\infty \mathcal{I}m \left\{ \int_{P^+} \bar{\Pi} \exp\left[-s\left(pr + \int_{x_3^R}^{x_3^S} \bar{\gamma}\, d\zeta \right) \right] dp \right\} dq, \tag{58}$$

which holds for both cases $\partial_p \tau|_{p_l} < 0$ and $\partial_p \tau|_{p_l} > 0$. If one deals with Green's functions that consist of both a part that is symmetical in q and a part that is antisymmetrical in q (e.g., $\hat{G}_{f_1}^{(0)-}$ and $\hat{G}_{f_2}^{(0)-}$), it is easily verified that the contribution from the latter part equals zero.

6.4 Replacing the variable of integration p by τ

If $\partial_p \tau|_{p_l} < 0$ the modified Cagniard contour intersects the real p-axis vertically at the point p_0. Progresssing along the contour away from p_0, τ monotonically increases. This means that we can straightaway replace the integration over the complex contour by an integration over the real parameter τ. The lowest value of τ is found in the point p_0 and is denoted by $T(q)$, which equals

$$T(q) = p_0 r + \int_{x_3^R}^{x_3^S} [c^{-2}(\zeta) - p_0^2 + q^2]^{1/2}\, d\zeta. \tag{59}$$

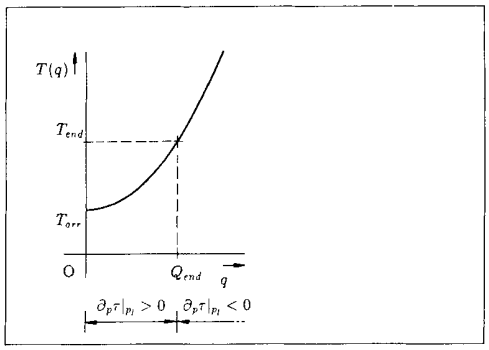

Figure 6. The function $T(q)$.

If for some value of q we have $\partial_p \tau|_{p_1} < 0$, then $p_0 < p_1$, and p_0 must be found numerically. If the horizontal offset r is large enough and the gradient of the wavespeed profile is not zero when reaching the maximum wavespeed on the interval $[x_3^R; x_3^S]$ (see Appendix A), there exists some $Q_{end} > 0$ such that for $0 \leq q < Q_{end}$ we have the condition $\partial_p \tau|_{p_1} > 0$. In this interval of q we simply find $p_0 = p_1$, while $T(q)$ follows from the equation

$$T(q) = (c_{max}^{-2} + q^2)^{1/2} r + \int_{x_3^R}^{x_3^S} [c^{-2}(\zeta) - c_{max}^{-2}]^{1/2} \, d\zeta. \tag{60}$$

In Fig. 6, $T(q)$ versus q has been drawn. The quantity $T(0)$ is the arrival time of the wave and will therefore be denoted by T_{arr}. Upon replacing the integration over p by an integration over τ, we obtain

$$\hat{G}_q^{(0)-} = \frac{-1}{2\pi^2} \int_0^\infty \int_{T(q)}^\infty \mathcal{I}m \, (\bar{\Pi} \, \partial_\tau p) \exp(-s\tau) \, d\tau \, dq. \tag{61}$$

Formally, if $q = Q_{end}$, we must interpret the outer integral as

$$\int_0^\infty \cdots dq = \lim_{\epsilon \downarrow 0} \left\{ \int_0^{Q_{end}-\epsilon} \cdots dq + \int_{Q_{end}+\epsilon}^\infty \cdots dq \right\} \tag{62}$$

to correctly treat the fact that $\partial_\tau p$ is not defined for $(q, \tau) = (Q_{end}, T_{end})$ because here we switch between the two types of contours. However, the contribution of the interval $[Q_{end} - \epsilon; Q_{end} + \epsilon]$ vanishes in the limit $\epsilon \downarrow 0$, which follows from the boundedness of the inner integral of equation (54) for every value of q. With this interpretation, we will still use the notation of equation (61). Moreover, with regard to equation (58) there is no need to distinguish between the cases $q > Q_{end}$ and $q < Q_{end}$, although they indicate different shapes of the modified Cagniard contour.

6.5 Reversing the order of integration and construction of the space–time domain Green's function

Let $q = Q(\tau)$ be the inverse of $\tau = T(q)$, then the interchanging of the order of integrations in equation (61) leads to

$$\hat{G}_q^{(0)-} = \frac{-1}{2\pi^2} \int_{T_{arr}}^\infty \int_0^{Q(\tau)} \mathcal{I}m \, (\bar{\Pi} \, \partial_\tau p) \exp(-s\tau) \, dq \, d\tau. \tag{63}$$

By inspection we find

$$G_q^{(0)-} = \frac{-1}{2\pi^2} H(t - T_{arr}) \int_0^{Q(t)} \mathcal{I}m \, (\bar{\Pi} \, \partial_t p) \, dq, \tag{64}$$

which is the desired space–time domain Green's function. Note that this result is simpler than we could have obtained when a Hankel transformation with respect to the horizontal coordinates had been used. In most cases the integral in equation (64) can easily be calculated numerically if some suitable substitution, e.g., $q = Q(t) \sin\theta$, is used to eliminate the inverse square root singularity due to $\partial_t p$ at $q = Q(t)$ if $Q(t) > Q_{end}$. For the configuration of Fig. 4 with specific parameter profiles as given in Fig. 7, the Green's function $G_q^{(0)-}$ has been shown in Fig. 8 for various values of the horizontal offset r. In this example the wavespeed and density of mass first increase with depth but, as opposed to the common situation, they decrease at larger depths; this represents a typical situation that can occur in the earth's crust. Although only piecewise linear parameter profiles have been used, which are the most elementary to describe a continuously layered medium, these profiles already necessitate the use of almost all features of our method. Only the situation that can give rise to a higher order zero in $\bar{\gamma}$, namely $\partial_3 c(x_3) = 0$ at $c(x_3) = c_{max}$, has not been incorporated. With our method a higher order zero, just like a first-order zero, will not influence the validity of the WKBJ iterative solution. Moreover, in that case it is easily proved (see Appendix A) that

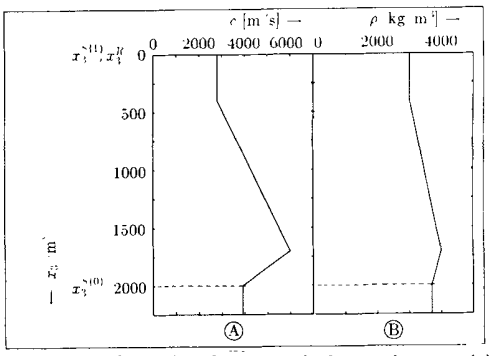

Figure 7. Parameter profile used to define a specific configuration for numerical experiments; (a) wavespeed profile; (b) mass density profile. Here, $x_3^{S(0)} = 2000$ m and $x_3^{S(1)} = 0$ m indicate the source levels that are used with the examples of the zeroth-order and first-order waves, respectively; the receiver level is always $x_3^R = 0$ m.

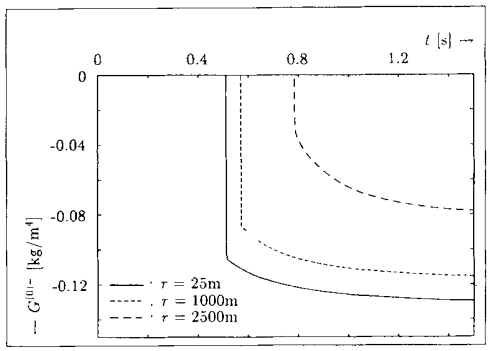

Figure 8. The Green's function $G_q^{(0)-}$ in our specific configuration for various values of the horizontal offset r.

always $\partial_\tau p|_{p_1} < 0$, so the points where $\tilde{\gamma}$ can have a higher order zero are never arrived at in the complex p-plane, so they do not cause any difficulties.

6.6 Convolution with the source signature

Referring to equation (48) and the theory of the Laplace transformation, the space–time domain acoustic pressure $p^{(0)-}$ due to a source of volume injection becomes

$$p^{(0)-} = \partial_t^2[Q^S(t) *_t G_q^{(0)-}(t)], \tag{65}$$

where $*_t$ indicates a convolution with respect to time. Taking a Blackman pulse with unit amplitude and a duration of 0.1 s as the source signature, the acoustic pressure at the receiver will be as in Fig. 9.

In the case where we have a source with other, or more, components than the volume injection $Q^S(t)$, their contribution is determined in the same manner as in the present section.

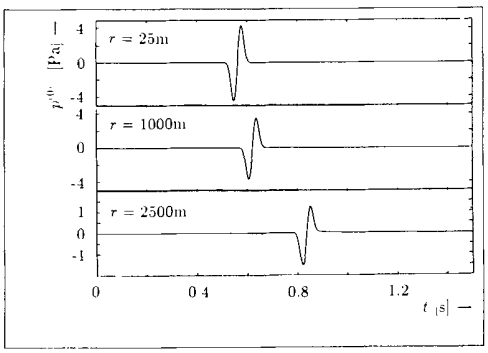

Figure 9. The acoustic pressure $p^{(0)-}$ for various values of the horizontal offset r.

7 TRANSFORMATION BACK TO THE SPACE–TIME DOMAIN: FIRST-ORDER COMPONENTS

Now that we have demonstrated the general applicability of the modified Cagniard method for the inversion of the zeroth-order components, we will use the same method for the inversion of the first-order components. Again the contour deformation will not influence the validity of our solution. Compared to the zeroth-order case there are two additional complications. To begin with, we have to perform an integration with respect to depth, since the first-order components are a continuous summation of partial reflections. These partial reflections, being dependent upon the reflection level, must first be transformed back to the space–time domain. This means that the inversion process becomes dependent upon depth too. Another complication is the possibility that the leftmost branch point is also a pole of the inhomogeneity function. Although Chapman (1974a, 1976) has also applied a version of the Cagniard method to transform the first-order components of a Neumann series solution back to the space–time domain, our approach differs significantly, mainly because of the continuous parameter profiles of general shape assumed.

We avoid the repetition of similar equations for all possible first-order components by explaining the inversion procedure for a first-order pressure wave, generated by continuous reflection of a downgoing zeroth-order order wave. This type of reflection is of major importance, e.g., in seismic prospecting. The corresponding configuration is shown in Fig. 10. Using the same notation as in the previous section, the pressure wave will be indicated by $p^{(1)-}$.

7.1 Introduction of first-order Green's functions

Upon applying the inverse Fourier transformation (6) to equation (42), we obtain $\hat{p}^{(1)-}$. To show the explicit dependence of the source signatures, we use Green's functions and write

$$\hat{p}^{(1)-} = s^2\hat{F}_1^S(s)\hat{G}_{f_1}^{(1)-} + s^2\hat{F}_2^S(s)\hat{G}_{f_2}^{(1)-} + s^2\hat{F}_3^S(s)\hat{G}_{f_3}^{(1)-} + s^2\hat{Q}^S(s)\hat{G}_q^{(1)-}. \tag{66}$$

The inversion procedure is the same for each first-order Green's function. We assume for brevity that the source is of the volume injection type only, and we will explain the inverse transformation process using the corresponding Green's function

$$\hat{G}_q^{(1)-} = \frac{-1}{8\pi^2}\int_{x_3^R}^{\infty}\int_{-\infty}^{\infty}\int_{-\infty}^{\infty}\chi(x_3)\Pi\exp\left[-s\vartheta(\alpha_1, \alpha_2, x_3)\right]d\alpha_1\, d\alpha_2\, dx_3, \tag{67}$$

with

$$\vartheta(\alpha_1, \alpha_2, x_3) = i\alpha_1 x_1 + i\alpha_2 x_2 + \int_{L(x_3)}\gamma\, d\zeta. \tag{68}$$

Here, $L(x_3)$ indicates the total vertical path from the source to the receiver; the integral over this path should be interpretated as

$$\int_{L(x_3)}\cdots d\zeta = \int_{x_3^S}^{x_3}\cdots d\zeta + \int_{x_3^R}^{x_3}\cdots d\zeta. \tag{69}$$

The inhomogeneity function $\chi(x_3)$ is explicitly given by

$$\chi(x_3) = -\frac{\partial_3 c(x_3)}{2c^3(x_3)\gamma^2(c_3)} - \frac{\partial_3\rho(x_3)}{2\rho(x_3)}. \tag{70}$$

7.2 Transformation of the variables α_1 and α_2 into p and q

First the variables α_1 and α_2, due to the occurrence of a 2-D Fourier transformation, will be transformed into p and q, according to equations (51) and (52). Now θ follows from the cylindrical coordinates of the receiver with respect to the source,

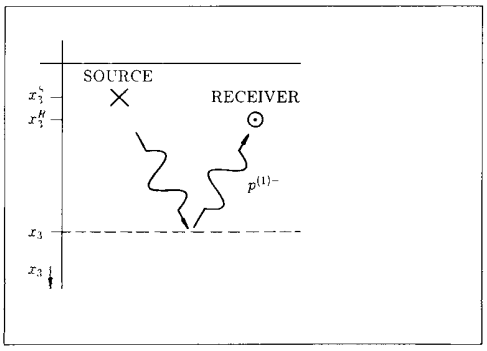

Figure 10. Configuration in which the first-order pressure wave propagates.

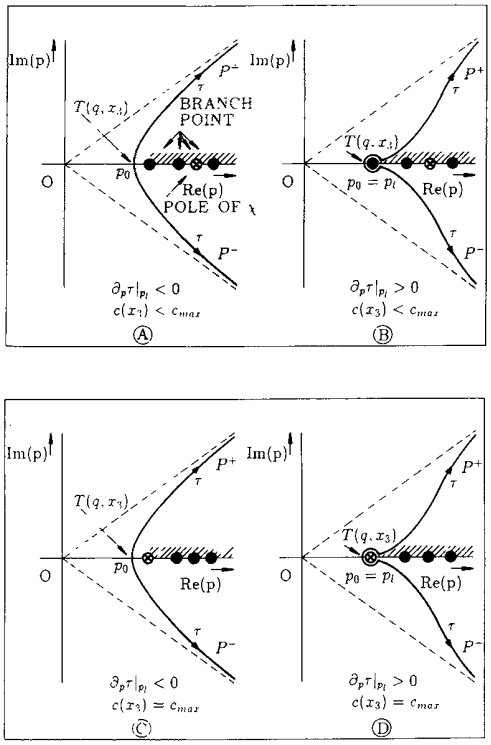

Figure 11. Possible locations of the modified Cagniard contour and the singularities in the right half of the complex p-plane. For cases (b) and (d) the detour around the branch point has already been made.

which are measured via the reflection level x_3,

$$r = \sqrt{(x_1^{\mathrm{R}})^2 + (x_2^{\mathrm{R}})^2}, \qquad \theta = \arctan\left(\frac{x_2^{\mathrm{R}}}{x_1^{\mathrm{R}}}\right), \qquad z = (x_2 - x_3^{\mathrm{S}}) + (x_3 - x_3^{\mathrm{R}}). \tag{71}$$

The variable r is the horizontal offset of the receiver, z is the length of the total vertical path $L(x_3)$. The equivalent of (67) is found by keeping p imaginary and q real, and is

$$\hat{G}_q^{(1)-} = \frac{i}{8\pi^2}\int_{x_3^{\mathrm{R}}}^{\infty}\int_{-\infty}^{\infty}\int_{-i\infty}^{i\infty}\bar{\chi}(x_3)\bar{\Pi}\exp\left[-s\left(pr + \int_{L(x_3)}\bar{\gamma}\,d\zeta\right)\right]dp\,dq\,dx_3. \tag{72}$$

In view of analytic continuation into the complex p-plane, we define $\mathcal{R}e\,(\bar{\gamma}) \geq 0$ in order to keep $\bar{\gamma}$ single valued. Branch points of the integrand in (72) are due to $\bar{\gamma}(x_3^{\mathrm{S}})$ and $\bar{\gamma}(x_3^{\mathrm{R}})$ in the denominator and to the integral of $\bar{\gamma}(\zeta)$ over $L(x_3)$ in the argument of the exponential function. The branch points of the latter integral are $p^{\mathrm{S}} = [c^{-2}(x_3^{\mathrm{S}}) + q^2]^{1/2}$, $p^{\mathrm{R}} = [c^{-2}(x_3^{\mathrm{R}}) + q^2]^{1/2}$, $p^{\chi} = [c^{-2}(x_3) + q^2]^{1/2}$, *and* the points $p^j = [c^{-2}(x_3^j) + q^2]^{1/2}$, with x_3^j on $L(x_3)$ $(j = 1, \ldots, n)$ forming the endpoints of the intervals where $\bar{\gamma}^j = [c^{-2}(\zeta) - (p^j)^2 + q^2]^{1/2}$ can be analytically continued into the complex ζ-plane. All branch points will be provided with branch cuts along the positive and negative real p-axis, respectively, from the relevant branch point to infinity. Contrary to the zeroth-order case, one pair of branch points also forms the poles of the inhomogeneity function. A clear distinction is to be made between two possible situations. The first occurs when the maximum wavespeed $c_{\max}$ on $L(x_3)$ is found somewhere *above* the reflection level x_3, so $c(x_3) < c_{\max}$. In this case two branch points that are not poles of the inhomogeneity function lie closest to the origin, see Fig. 11(a) and (b). In the second situation the maximum wavespeed is found *at* the reflection level, so $c(x_3) = c_{\max}$. It is clear that this can only happen if the wavespeed profile has a non-negative first derivative here. In this case two branch points that are poles of the inhomogeneity function lie closest to the origin, see Fig. 11(c) and (d). In view of the application of Jordan's lemma, the deformation is only allowed to take place in the right half of the p-plane.

7.3 The modified Cagniard path

The path of integration is deformed into the modified Cagniard path defined by

$$\tau = pr + \int_{L(x_3)}\bar{\gamma}(\zeta)\,d\zeta, \tag{73}$$

where τ is always kept real. According to Appendix A, the sign of the quantity

$$\partial_p \tau|_{p_1} = r - p_1 \int_{L(x_3)} [c^{-2}(\zeta) - p_1^2 + q^2]^{-1/2}\, d\zeta \tag{74}$$

indicates the type of modified Cagniard contour. Here, $p_1 = p_1(q, x_3) = (c_{\max}^{-2} + q^2)^{1/2}$, with $c_{\max} = \max_{\zeta \in L(x_3)} \{c(\zeta)\}$, indicates the leftmost branch point. If $\partial_p \tau|_{p_1} < 0$, the complex part of the countour crosses the real p-axis vertically at a point p_0 to the left of p_1, so there is no interference with the branch cuts. If $\partial_p \tau|_{p_1} > 0$, *a case which is impossible for piecewise homogeneous configurations,* the complex part of the contour meets the real axis horizontally in $p_0 = p_1$, which is either a normal branch point *or also a pole of the inhomogeneity function.* In Appendix B the shape of the modified Cagniard contour is related to the shape of the generalized ray associated with the point p_0. Here $\partial_p \tau|_{p_1}$, if greater than zero, is the length of the sum of both horizontal parts of a ray; if $\partial_p \tau|_{p_1} < 0$ the ray does nowhere have a horizontal trajectory. The ray paths associated with first-order waves never extend beyond the vertical interval $[x_3^S; x_3] \cup [x_3^R; x_3]$.

In the same way as in the previous section we can show that the integration along the imaginary p-axis can be replaced by an integration along the modified Cagniard contour. As we can see in Fig. 11(a) and (c), if $\partial_p \tau|_{p_1} < 0$, no special precautions have to be taken. But if $\partial_p \tau|_{p_1} > 0$ the modified Cagniard contour must be supplemented by a small circle with radius $\delta > 0$ in order to go around the singularity. If in this case $c(x_3) < c_{\max}$, as in Fig. 11(b), in the limit $\delta \to 0$ this circle gives a vanishing contribution to the total integral. However, if $c(x_3) = c_{\max}$ we arrive at the situation of Fig. 11(d), where this circle gives a non-zero contribution to the total integral in the limit $\delta \to 0$. From now on the various situations will be referred to by the corresponding letter shown in Fig. 11. The contour is symmetrical with respect to the real p-axis and the integrand satisfies Schwarz' reflection principle; further the integrand is symmetrical with respect to q. Hence, we can rewrite equation (72) as

$$\hat{G}_q^{(1)-} = \begin{cases} \dfrac{-1}{2\pi^2} \displaystyle\int_{x_3^R}^{\infty} \int_0^{\infty} \mathcal{I}m \left[\int_{P^+} \bar{\chi}(x_3) \bar{\Pi} \exp(-s\tau)\, dp \right] dq\, dx_3, & \text{cases (a), (b), (c),} \\ \dfrac{-1}{2\pi^2} \displaystyle\int_{x_3^R}^{\infty} \int_0^{\infty} \mathcal{I}m \left[\int_{P^+} \bar{\chi}(x_3) \bar{\Pi} \exp(-s\tau)\, dp \right] dq\, dx_3 + \dfrac{1}{2\pi} \int_{x_3^R}^{\infty} \int_0^{\infty} \mathrm{Res}_{p=p_1} [\bar{\chi}(x_3) \bar{\Pi} \exp(-s\tau)]\, dq\, dx_3, & \text{case (d).} \end{cases} \tag{75}$$

7.4 Replacing the variable of integration p by τ

The integration over the complex contour is replaced by an integration over the real parameter τ. The lowest value of τ is found in the point p_0 and is denoted by $T(q, x_3)$, which equals

$$T(q, x_3) = p_0 r + \int_{L(x_3)} [c^{-2}(\zeta) - p_0^2 + q^2]^{1/2}\, d\zeta. \tag{76}$$

For the contours in Fig. 11(a) and (c), we have $p_0 < p_1$ and p_0 must be found numerically. The contours in Fig. 11(b) and (d) show up if the horizontal offset r is large enough and the gradient of the wavespeed profile is not zero at the point where $c(x_3) = c_{\max}$. If these requirements are met, we have for $0 \le q < Q_{\text{end}}(x_3)$ the condition $\partial_p \tau|_{p_1} > 0$, resulting in $p_0 = p_1$, while $T(q, x_3)$ follows from the equation

$$T(q, x_3) = (c_{\max}^{-2} + q^2)^{1/2} r + \int_{L(x_3)} [c^{-2}(\zeta) - c_{\max}^{-2}]^{1/2}\, d\zeta. \tag{77}$$

Graphs equivalent to Fig. 6 can now be made for every value of x_3. The quantity $T(0, x_3)$ is also denoted as $T_{\text{arr}}(x_3)$ because it represents the arrival time of the wave reflected at the vertical level x_3. If both conditions $q \le Q_{\text{end}}(x_3)$ and $c(x_3) = c_{\max}$ are met, we have case (d) and we must add the term due to the residue of the branch point that also forms the pole of the inhomogeneity function. In view of later manipulations it will be more convenient to replace the first condition by $T_{\text{arr}}(x_3) \le \tau \le T_{\text{end}}(x_3)$. As a consequence, unlike the zeroth-order case, we have to determine $T_{\text{end}}(x_3)$. Because this quantity is connected with the contour that forms the limit between the two types, it can be found by combining the equations

$$p_0 = p_1 = (c_{\max}^{-2} + q^2)^{1/2}, \tag{78}$$

$$r - p_0 \int_{L(x_3)} [c^{-2}(\zeta) - p_0^2 + q^2]^{-1/2}\, d\zeta = 0, \tag{79}$$

$$T_{\text{end}}(x_3) = p_0 r + \int_{L(x_3)} [c^{-2}(\zeta) - p_0^2 + q^2]^{1/2}\, d\zeta. \tag{80}$$

After some simple manipulations we find

$$T_{\text{end}}(x_3) = r^2 \left\{ \int_{L(x_3)} [c^{-2}(\zeta) - c_{\max}^{-2}]^{-1/2}\, d\zeta \right\}^{-1} + \int_{L(x_3)} [c^{-2}(\zeta) - c_{\max}^{-2}]^{1/2}\, d\zeta. \tag{81}$$

Note that the quantities T_{arr} and T_{end} are dependent on the vertical reflection level x_3, but independent of q. Equation (81) has no meaning if $T_{\text{end}}(x_3) < T_{\text{arr}}(x_3)$.

In the residual part of equation (75) we can restrict the interval of the q-integration to $[0; Q_{\text{end}}(x_3)]$ since outside this interval the contour does not meet the leftmost singularity and the residue will always be zero. Within this interval, the residue is not equal to zero if $c(x_3) = c_{\max}$. Defining the function

$$S(x_3) = \begin{cases} 0 & \text{if } c(x_3) < c_{\max}, \\ 1 & \text{if } c(x_3) = c_{\max}, \end{cases} \tag{82}$$

the residue is found to be

$$\begin{aligned} \text{Res}_{p=p_1}(\cdots) &= \frac{S(x_3)\,\partial_3 c(x_3) \exp\left[-sT(q, x_3)\right]}{4c_{\max}^2 (c_{\max}^{-2} + q^2)^{1/2} [c^{-2}(x_3^{\text{S}}) - c_{\max}^{-2}]^{1/4} [c^{-2}(x_2^{\text{R}}) - c_{\max}^{-2}]^{1/4}} \\ &= R(q, x_3) \exp\left[-sT(q, x_3)\right]. \end{aligned} \tag{83}$$

In the non-residual and residual parts of (75) we let integrations over τ replace the integrations over p and q, respectively, resulting in

$$\begin{aligned} \hat{G}_q^{(1)-} = &\frac{-1}{4\pi^2} \int_{x_3^{\text{R}}}^{\infty} \int_{-\infty}^{\infty} \int_{T_{\text{arr}}(x_3)}^{\infty} \mathcal{I}m\,(\bar{\chi} \bar{\Pi}\, \partial_\tau p) \exp(-s\tau)\, d\tau\, dq\, dx_3 \\ &+ \frac{1}{2\pi} \int_{x_3^{\text{R}}}^{\infty} S(x_3) \int_{T_{\text{arr}}(x_3)}^{T_{\text{end}}(x_3)} R[Q(\tau, x_3), x_3] \exp(-s\tau)\, \partial_\tau Q(\tau, x_3)\, d\tau,\, dx_3. \end{aligned} \tag{84}$$

Here $q = Q(\tau, x_3)$ is the inverse of $\tau = T(q, x_3)$ with respect to the first argument. Just like the previous section there is no need to use the formal limiting process when evaluating the integrals with respect to q around $q = Q_{\text{end}}(x_3)$.

7.5 Reversing the order of integration and construction of the space–time domain Green's function

We will cast the different parts of equation (84) into a form from which the space–time domain Green's function can be recognized. First we reverse the order of integration in the first term of $\hat{G}_q^{(1)-}$. This leads to

$$\begin{aligned} \hat{G}_q^{(1)-} = &\frac{-1}{2\pi^2} \int_{x_3^{\text{R}}}^{\infty} \int_{T_{\text{arr}}(x_3)}^{\infty} \int_0^{Q(\tau, x_3)} \mathcal{I}m\,[\bar{\chi}(x_3) \bar{\Pi}\, \partial_\tau p] \exp(-s\tau)\, dq\, d\tau\, dx_3 \\ &+ \frac{1}{2\pi} \int_{x_3^{\text{R}}}^{\infty} S(x_3) \int_{T_{\text{arr}}(x_3)}^{T_{\text{end}}(x_3)} R[Q(\tau, x_3), x_3] \exp(-s\tau)\, \partial_\tau Q(\tau, x_3)\, d\tau\, dx_3. \end{aligned} \tag{85}$$

The space–time domain Green's function $G_q^{(1)-}$ can now be recognized as

$$\begin{aligned} G_q^{(1)-} = &\frac{-1}{2\pi^2} \int_{x_3^{\text{R}}}^{\infty} H[t - T_{\text{arr}}(x_3)] \int_0^{Q(t, x_3)} \mathcal{I}m\,[\bar{\chi}(x_3) \bar{\Pi}\, \partial_t p]\, dq\, dx_3 \\ &+ \frac{1}{2\pi} \int_{x_3^{\text{R}}}^{\infty} S(x_3) H[t - T_{\text{arr}}(x_3)] H[T_{\text{end}}(x_3) - t] R[Q(t, x_3), x_3]\, \partial_t Q(t, x_3)\, dx_3. \end{aligned} \tag{86}$$

The numerical evaluation of the integrals with respect to q in equation (86) will in general be simplified by some suitable substitution, e.g., $q = Q(t, x_3) \sin\theta$. Numerical experiments have been performed using the configuration of Fig. 10 with specific parameter profiles as presented in Fig. 7. In Fig. 12 we have plotted the functions $T_{\text{arr}}(x_3)$ and $T_{\text{end}}(x_3)$ versus x_3. In a numerical implementation of (86) these functions are used to determine the vertical intervals in which cases (b) or (d) can show up. The Green's function $G_q^{(1)-}$ has been shown in Fig. 13 for various values of the horizontal offset r. The sharp peak in Green's function for $r = 5000$ m has a logarithmic nature and can be associated with a caustic in ray theory. Although the parameter profiles are simple linear functions, almost all features of our method must be used. Only the situation that can give rise to a higher order zero in $\bar{\gamma}$, namely $\partial_3 c(x_3) = 0$ at $c(x_3) = c_{\max}$, has not been covered, but we can prove that the method does not break down at such points.

7.6 Convolution with the source signature

Using equation (66) and the theory of the Laplace transformation, we find that the space–time domain acoustic pressure $p^{(1)-}$ due to a source of volume injection becomes

$$p^{(1)-} = \partial_t^2 [Q^{\text{S}}(t) *_t G_q^{(1)-}(t)]. \tag{87}$$

Using a Blackman pulse with unit amplitude and a duration of 0.1 s as the source signature, the acoustic pressure at the

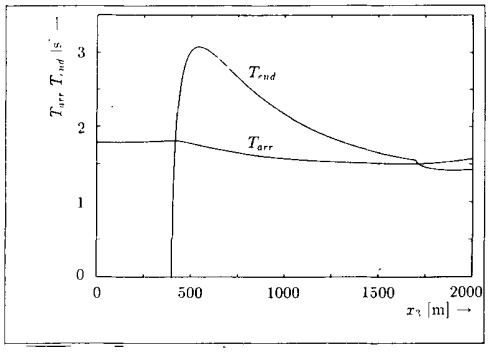

Figure 12. The functions $T_{arr}(x_3)$ and $T_{end}(x_3)$.

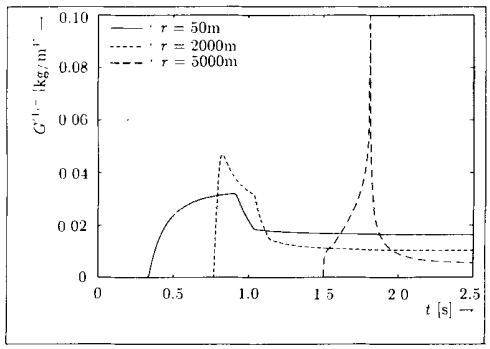

Figure 13. The Green's function $G_q^{(1)-}$ in our specific configuration for various values of the horizontal offset r.

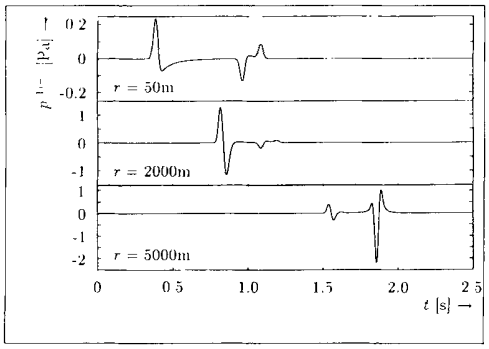

Figure 14. The pressure $p^{(1)-}$ for various values of the horizontal offset r.

receiver will be as shown in Fig. 14. An analogous version of the method presented in this section can be used when we have a source with other, or more, components than the volume injection $Q^S(t)$. In principle, the inversion of higher order terms is conducted along the same lines as in this section. However, the numerical evaluation of higher order components will involve an increasing amount of effort. This problem can be partly circumvented by applying an approximate version of our method for these higher order components. The problems related to multiple poles of the inhomogeneity function can be treated by an alternative approach, which is explained in Appendix D.

8 CONCLUSIONS

We have presented a method which in principle gives an exact solution of the wave propagation problem in a horizontally, continuously layered configuration with arbitrary parameter profiles. Using a Laplace transformation with respect to the time coordinate, causality can be ensured throughout the derivation. After applying a 2-D Fourier transformation with respect to the horizontal coordinates, we have solved the resulting transform-domain differential equation using a Neumann series or WKBJ iterative solution. Physically, each term in the solution consists of a continuous summation of contributions that have undergone a specific number of partial reflections. Owing to the use of the Laplace transformation, both the transform-domain solution and the resulting space–time domain solution are convergent iterative solutions for any configuration. Using the modified Cagniard method for the transformation back to the space–time domain, this convergence has been preserved. We

have seen that this relies on Cauchy's theorem, according to which we may deform an integration path as a part of the inverse transformation process and still obtain the same result as before the deformation, provided we have taken care to prevent the deformed path to pass any singularities. As a result, first-order and higher order zeroes of the propagation coefficient, which cannot be present along the original paths of integration, can be dealt with. Moreover, the points where the propagation coefficient has a higher order zero are not reached by the deformed contour anyway. The inverse transformation method has been demonstrated by deriving closed-form, space–time domain expressions for components of the first two terms of the WKBJ iterative solution. Attention has been paid to make the method mathematically straightforward. The modified Cagniard contour is in general to be determined numerically, for which an input routine that describes the parameter profiles by piecewise analytical functions is needed. Numerical results for two canonical configurations have been included.

During the derivation of the theory we have come across some important points. The most important of these is the convergence of the solution in any continuously layered configuration, making the method generally applicable. Connected to the modified Cagniard method is the fact that, unlike other methods, the intermediate quantities are related with a real time variable, so in this respect they are physical. Further we have investigated the (generalized) ray paths that are associated with the wavefronts of the components. With the present method a turning ray is considered as a special case of a reflected ray. As a result, the rays belonging to the first term of the series show no turning point, but turning rays can occur for higher order terms. Besides turning rays which are only horizontal at a single point, we also have observed rays which travel horizontally over non-zero distances. From Appendices A and B it follows that there are no rays which have a horizontal part, not even at one single point, on a vertical level where the wavespeed profile has a zero first derivative. It has not been necessary to introduce the notion of tunnelling in our theory. Although in certain aspects our rays differ from those more commonly encountered in literature, we note that our rays are associated with a real, i.e., physical, time parameter.

ACKNOWLEDGMENTS

The research reported in this paper has been financially supported through research grants from the Stichting Fund for Science, Technology and Research (a companion organization to the Schlumberger Foundation in the USA), from Schlumberger–Doll Research, Ridgefield, CT, USA, from Etudes et Productions Schlumberger, Clamart, France, and from the Royal/Dutch Shell Exploration and Production Laboratories, Rijswijk, The Netherlands. This support is gratefully acknowledged.

REFERENCES

Achenbach, J. D., 1973. *Wave Propagation in Elastic Solids*, North Holland, Amsterdam.

Aki, K. & Richards, P. G., 1980. *Quantitative Seismology: Theory and Methods*, W. H. Freeman, San Francisco.

Backus, G. E. & Mulcahy, M., 1976. Moment tensors and other phenomenological descriptions of seismic sources—I. Continuous displacements, *Geophys. J. R. astr. Soc.*, **46**, 341–361.

Ben-Menahem, A. & Singh, S. J., 1981. *Seismic Waves and Sources*, Springer-Verlag, New York.

Bremmer, H., 1939. Geometrisch-optische benadering van de golfvergelijking, in *Handelingen Natuur- en Geneeskundig Congres, Nijmegen*, pp. 88–91, Ruygrok, Haarlem, The Netherlands (in Dutch).

Bremmer, H., 1951. The W.K.B. approximation as the first term of a geometric–optical series, *Comm. Pure appl. Math.*, **4**, 105–115. Also in *The Theory of Electromagnetic Waves*, pp. 169–179, ed. Kline, M., The Interscience Publishers, New York.

Budden, K. G., 1961. *Radio Waves in the Ionosphere*, Cambridge University Press, Cambridge.

Cagniard, L., 1939. *Réflection et Réfraction des Ondes Seismiques Progressives*, Gauthier-Villars, Paris (in French). Translated and revised version: Flinn, E. A. & Dix, C. H., 1962. *Reflection and Refraction of Progressive Seismic Waves*, McGraw-Hill, New York.

Chapman, C. H., 1974a. Generalized ray theory for an inhomogeneous medium, *Geophys. J. R. astr. Soc.*, **36**, 673–704.

Chapman, C. H., 1974b. The turning point of elastodynamic waves, *Geophys. J. R. astr. Soc.*, **39**, 613–621.

Chapman, C. H., 1976. Exact and approximate generalized ray theory in vertically inhomogeneous media, *Geophys. J. R. astr. Soc.*, **46**, 201–233.

Chapman, C. H., 1978. A new method for computing synthetic seismograms, *Geophys. J. R. astr. Soc.*, **54**, 481–518.

Chapman, C. H., 1981. Long-period corrections to body waves: Theory, *Geophys. J. R. astr. Soc.*, **64**, 321–372.

Chapman, C. H. & Orcutt, J. A., 1985. The computation of body wave synthetic seismogams in laterally homogeneous media, *Rev. Geophys.*, **23**, 105–163.

Choy, G. L., 1977. Theoretical seismograms of core phases calculated by frequency-dependent full wave theory and their interpretation, *Geophys. J. R. astr. Soc.*, **51**, 275–311.

De Hoop, A. T., 1960. A modification of Cagniard's method for solving seismic pulse problems, *Appl. Sci. Res.*, **B8**, 349–356.

De Hoop, A. T., 1961. Theoretical determination of the surface motion of a uniform elastic half-space produced by a dilatational, impulsive, point source, in *Proceedings Colloque International du CNRS*, no. 111, pp. 21–30, Marseille.

De Hoop, A. T., 1988. Acoustic radiation from impulsive sources in a layered fluid, *Nieuw Archief voor Wiskunde*, **6**, 111–129.

De Hoop, A. T., 1990. Acoustic radiation from an impulsive point source in a continuously layered fluid—An analysis based upon the Cagniard method, *J. Acoust. Soc. Am.*, in press.

Garmany, J., 1988a. Seismograms in stratified anisotropic media—I. WKBJ theory, *Geophys. J. R. astr. Soc.*, **92**, 365–377.

Garmany, J., 1988b. Seismograms in stratified anisotropic media—II. Uniformly asymptotic approximations. *Geophys. J. R. astr. Soc.*, **92**, 379–389.

Helmberger, D. V., 1968. The crust–mantle transition in the Bering Sea, *Bull. seism. Soc. Am.*, **58**, 179–214.

Heyman, E. & Felsen, L. B., 1984. Non-dispersive approximations for transient ray fields in an inhomogeneous medium, in *Proceedings of the NATO Advanced Research Workshop on Hybrid Formulation of Wave Propagation and Scattering*, pp. 269–284, ed. Felsen, L. B., Martinus Nijhoff Publishers, Dordrecht.

Kennett, B. L. N., 1983. *Seismic Wave Propagation in Stratified Media*, Cambridge University Press, Cambridge.

Kennett, B. L. N. & Illingworth, M. R., 1981. Seismic waves in a stratified half space—III. Piecewise smooth models, *Geophys. J. R. astr. Soc.*, **66**, 633–675.

Langer, R. E., 1937. On the connection formulas and the solution of the wave equation, *Phys. Rev., Ser. 2*, **51**, 669–676.

Morse, P. M. & Feshbach, H., 1953. *Methods of Theoretical Physics*, McGraw-Hill, New York.

Müller, G., 1970. Exact ray theory and its application to the reflection of elastic waves form vertically inhomogeneous media, *Geophys. J. R. astr. Soc.*, **21**, 261–283.

Pao, Y. H. & Gajewski, R. R., 1977. The generalized ray theory and transient responses of layered elastic solids, *Phys. Acoust.*, **13**, 183–265.

Spencer, T. W., 1960. The method of generalized reflection and transmission coefficients, *Geophysics*, **25**, 625–641.

Van der Hijden, J. H. M. T., 1987. *Propagation of Transient Elastic Waves in Stratified Anisotropic Media*, North Holland, Amsterdam.

Wasow, W., 1965. *Asymptotic Expansion of Ordinary Differential Equations*, vol. 14, Pure and Applied Mathematics, Wiley, New York.

Widder, D. V., 1946. *The Laplace Transform*, Princeton University Press, Princeton, NJ.

Wiggins, R. A. & Helmberger, D. V., 1974. Synthetic seismogram computation by expansion in generalized rays, *Geophys. J. R. astr. Soc.*, **37**, 73–90.

APPENDIX A: PROPERTIES OF THE MODIFIED CAGNIARD PATHS FOR CONTINUOUSLY LAYERED MEDIA

The modified Cagniard contour consists of the points in the complex p-plane for which

$$\tau = pr + \int_L \bar{\gamma}(\zeta)\, d\zeta, \tag{88}$$

yields a real value. In this equation p is the horizontal slowness, r is the horizontal offset and $\bar{\gamma}(x_3) = [c^{-2}(x_3) - p^2 + q^2]^{1/2}$ is the propagation coefficient or vertical slowness. We use L to indicate the total vertical integration path. The branch points $p^j = [c^{-2}(x_3^j) + q^2]^{1/2}$ of the integral in equation (88) can be arranged in two groups. The first group contains branch points in which x_3^j equals x_3^S and x_3^R and the points of reflection $x_3, x_3', \ldots, x_3^{(k)}$. The branch points of the second group are due to $x_3^j = x_3^a, \ldots, x_3^n$ on L that form the endpoints of the intervals where $\bar{\gamma}^j(\zeta) = [c^{-2}(\zeta) - (p^j)^2 + q^2]^{1/2}$ can be analytically continued into the complex ζ-plane. [Note that it is a consequence of Cauchy's theorem that only these endpoints determine the result of the integral in (88).] Although in the left half of the p plane there are trajectories that satisfy equation (88), we restrict our considerations to the right half of the p-plane, because in view of Jordan's lemma in this region contour deformation will take place.

First, we define the quantity $p_1 = p_1(q) = (c_{\max}^{-2} + q^2)^{1/2}$, with $c_{\max} = \max_{x_3 \in L} \{c(x_3)\}$, the leftmost branch point. Although the real axis between $p = 0$ and $p = p_1$ satisfies equation (88), in general the path of integration will be deformed into a modified Cagniard contour that consists of the complex values that satisfy equations (88). For large values of τ this complex path approaches asymptotically the straight lines

$$p \sim \frac{\tau}{r - iz} \tag{89}$$

as $\tau \to \infty$ in the first quadrant of the p-plane,

$$p \sim \frac{\tau}{r + iz} \tag{90}$$

as $\tau \to \infty$ in the fourth quadrant of the p-plane, where z denotes the toal length of the vertical path from source to receiver. Note that these asymptotes are independent of q. In continuously layered configurations the modified Cagniard contour can approach the real axis in two distinct ways. These depend upon the values of the quantity

$$\partial_p \tau|_{p_1} = r - (c_{\max}^{-2} + q^2)^{1/2} \int_L [c^{-2}(\zeta) - c_{\max}^{-2}]^{-1/2}\, d\zeta. \tag{91}$$

The first possibility, that is also encountered in (piecewise) homogeneous configurations, occurs if $\partial_p \tau|_{p_1} < 0$. Since $\partial_p \tau|_{p=0} = r > 0$ and $\partial_p \tau$ is continuously decreasing on the interval $[0; p_1\rangle$ as the expression for $\partial_p \tau$ derived from (88) shows, there must be some point p_0, with $0 \le p_0 < p_1$, for which $\partial_p \tau|_{p_0} = 0$. Travelling along the real axis, τ has a maximum value in this point, while travelling along the modified Cagniard contour τ has its minimum value. Thus the point p_0 is a saddle point in the complex p-plane, and the complex contour crosses the real axis perpendicularly. Fig. 5(a) shows an example of this type of modified Cagniard contour.

As opposed to the (piecewise) homogeneous case, we can for continuously layered configurations sometimes have $\partial_p \tau|_{p_1} > 0$. In this case, τ will monotonically increase along the real axis from $p = 0$ to $p = p_1$. For $p > p_1$, τ certainly becomes complex, so this part of the real axis will not be a candidate for the modified Cagniard contour. Moreover, $\lim_{p \to p_1} \partial_p \tau$ is real

valued, and we conclude that now the complex contour meets the real p-axis tangentially in p_1. An example of this type of modified Cagniard contour is shown in Fig. 5(b).

Next we investigate how the contour type depends upon the configuration. We note that for every $\delta > 0$ it is possible to define vertical intervals ϵ_i on which $|c(x_3) - c_{\max}| < \delta$ and the wavespeed profile can be considered linear. On the remaining part of L the quantity $[c^{-2}(x_3) + q^2]^{1/2}$ is bounded away from p_1, and the contribution of this part will be finite. Using some simple mathematics we can prove that the contribution of the intervals ϵ_i to the integral in equation (91) is finite if $\partial_3 c(x_3) \neq 0$ in $c_{\max}$. As a result we can state that for continuously layered media it is possible to have $\partial_p \tau|_{p_1} > 0$, provided r is large enough and the wavespeed profile does not have a zero first derivative at $c_{\max}$.

If somewhere $\partial_3 c(x_3) = 0$ in $c_{\max}$, the linear interpolation function must be replaced by a quadratic function, and it can be shown that the contribution of the respective interval ϵ_i to the integral in equation (91) is now infinite. Inversely we may conclude that if $\partial_p \tau|_{p_1} > 0$, the wavespeed profile will not have a stationary point at $c_{\max}$, but $c_{\max}$ is reached either on a vertical level where the first derivative of the wavespeed profile is discontinuous, or at some boundary of the intervals $[x_3^S; x_3], [x_3; x_3'], \ldots, [x_3^{(k)}; x_3^R]$.

Finally we note that a linear interpolation function is the most simple function that conserves the continuous character of the profile. Theoretically speaking a piecewise constant interpolation function is not satisfactory as the continuous character is lost and the possibility $\partial_p \tau|_{p_1} > 0$ is not encountered.

APPENDIX B: RAY SHAPES

As we have seen in Appendix A, the modified Cagniard contour meets the real p-axis in the point p_0. Here, τ has its minimum value on the contour, and is denoted by T_{arr}, which reflects the fact that at this time instant the first disturbance due to the observed wave phenomenon arrives at the receiver. Since the complete set of points up to where the first disturbance of a wave phenomenon has arrived is the wavefront, and rays are defined as lines connecting equivalent points on successive wavefronts, we can state that T_{arr} is the time needed to go from the source to the receiver along a ray. In this appendix we investigate the relation between the behaviour of the modified Cagniard contour in p_0 and the shape of the corresponding ray.

In Fig. 15(a) we see a ray in a continuously layered medium (without loss of generality in this appendix we take $x_2 = 0$ and $q = 0$). Along any ray segment $d\vec{s}$ we have a horizontal slowness p_1 and a vertical slowness p_3. Because the medium is isotropic, the vertical slowness is related to the horizontal slowness by

$$p_3 = [c^{-2}(x_3) - p_1^2]^{1/2}. \tag{92}$$

As a result, the total time needed to travel from A to B along the ray equals

$$T_{\text{arr}} = \int_0^r p_1 \, dx_1 + \int_L [c^{-2}(x_3) - p_1^2]^{1/2} \, dx_3, \tag{93}$$

where L is the total vertical path; here it equals $[x_3^A; x_3^B]$. Note that integration over one coordinate does not mean that the other coordinate can be chosen arbitrarily, as both coordinates are coupled via the ray path.

Next we turn our attention to the modified Cagniard contour, which in any case yields

$$T_{\text{arr}} = p_0 r + \int_L [c^{-2}(\zeta) - p_0^2]^{1/2} \, d\zeta. \tag{94}$$

Independently of r and L, equations (93) and (94) must yield equal results. As a consequence, we find the identity $p_1 = p_0$,

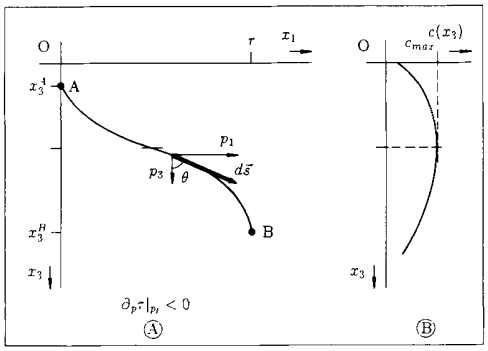

Figure 15. (a) Ray in a continuously layered configuration; (b) wavespeed profile of the medium.

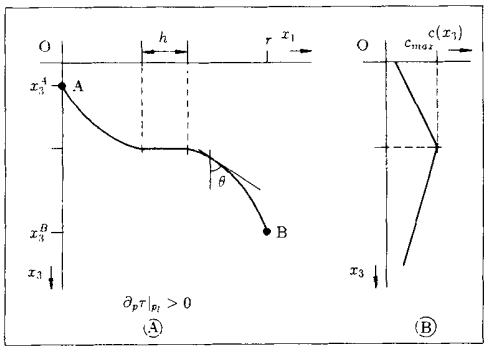

Figure 16. Ray with a horizontal part.

which is constant for a given ray. Moreover, looking at Fig. 15 we can easily see that

$$\frac{\sin\theta(x_3)}{c(x_3)} = p_1, \tag{95}$$

and since $p_1 = p_0 =$ constant for each ray this yields Snell's law.

From Appendix A we know that for $\partial_p\tau|_{p_1} < 0$ the point p_0 is situated to the left of the point $p_1 = 1/c_{max}$, with $c_{max} = \max_{x_3 \in L}\{c(x_3)\}$. In this case Snell's law shows that $\theta(x_3) < \pi/2$, so the associated ray will nowhere have a horizontal trajectory. However, if $\partial_p\tau|_{p_1} > 0$, we have $p_0 = p_1 = 1/c_{max}$, and $\theta(x_3)$ can have a horizontal part, see Fig. 16. Thus we can state that the type of Cagniard contour indicates whether the associated ray has a horizontal part or not.

The time needed to travel from A to B along the ray in Fig. 16 equals

$$T_{arr} = \int_L p_3\,dx_3 + \int_0^r p_1\,dx_1 = \int_L \{[c^{-2}(x_3) - p_1^2]^{1/2} + p_1\tan\theta(x_3)\}\,dx_3 + hp_1, \tag{96}$$

where h is the horizontal path length of the ray. Differentiation of equation (96) with respect to p yields

$$\partial_p\tau|_{p_1} = \int_L \{-p_1[c^{-2}(x_3) - p_1^2]^{-1/2} + \tan\theta(x_3)\}\,dx_3 + h = h, \tag{97}$$

so at this stage we can summarize that the quantity $\partial_p\tau|_{p_1}$, if greater than zero, indicates the length of the horizontal part of a ray, whereas a negative value means that the ray does nowhere have a horizontal trajectory.

The modified Cagniard contour associated with a ray that does not travel horizontally anywhere, has $\partial_p\tau = 0$ in p_0, the point where τ equals T_{arr}. So this ray forms a path from the source to the receiver for which the traveltime is stationary, according to the present-day version of Fermat's principle. However, for the modified Cagniard contour related to a ray with a horizontal part we find $\partial_p\tau > 0$ in $p_0 = p_1$. The value T_{arr} in this point is not a stationary value of τ, although it reaches its minimum value. It is an interesting fact that in this respect the rays with a horizontal part still satisfy the original version of Fermat's principle (rays are the paths with the least traveltime), but not the present-day version.

Although we have restricted our investigation to a simple ray belonging to a zeroth-order wave component, the same discussion can be held for rays with one or more reflection points. We can think of these rays as if they were composed of parts like those already treated. If reflection takes place at the vertical levels $x_3, x_3', \ldots, x_3^{(k)}$, the total vertical path L consists of the union of the intervals $[x_3^S; x_3]$, $[x_3; x_3']$, $\ldots$, $[x_3^{(k)}; x_3^R]$, while $\partial_p\tau|_{p_1}$ indicates the total length of a number of horizontal parts of the ray.

APPENDIX C: EQUATIONS FOR ISOTROPIC, ELASTIC MEDIA

The method presented in this paper can also be used in the case of wave propagation in continuously layered elastic media. Here we will show the changes that are necessary with respect to the acoustical case, and we will see that neither of these prohibits the application of our method. In this appendix we use the notation of Van der Hijden (1987). To start with, the space–time domain linearized elastic equations are

$$\partial_j\tau_{ij} - \rho_{ij}(x_3)\,\partial_t v_j = -f_i, \tag{98}$$

$$\tfrac{1}{2}(\partial_i v_j + \partial_j v_i) - s_{ijpq}(x_3)\,\partial_t\tau_{pq} = h_{ij}, \tag{99}$$

where τ_{ij} is the stress, v_j is the particle wavespeed, f_i is the volume density of volume force and h_{ij} is the volume density of strain rate. Although it has not been indicated explicitly, the action of a moment tensor M_{ij} (Backus & Mulcahy 1976) can be incorporated in the source by adding a term $\partial_j M_{ij}$ to the right-hand side of equation (98). We assume the presence of a

point-source for which, without loss of generality,

$$\{f_i(x_k, t), h_{ij}(x_k, t)\} = \{F_i^S(t), H_{ij}^S(t)\}\, \delta(x_1, x_2, x_3 - x_3^S). \tag{100}$$

The medium properties are described by the tensors of the volume density of mass

$$\rho_{ij}(x_3) = \rho(x_3)\, \delta_{ij}, \tag{101}$$

and the compliance

$$s_{ijpq}(x_3) = \frac{-\lambda(x_3)}{2\mu(x_3)[3\lambda(x_3) + 2\mu(x_3)]}\, \delta_{ij}\, \delta_{pq} + \frac{1}{4\mu(x_3)}(\delta_{ip}\, \delta_{jq} + \delta_{iq}\, \delta_{jp}). \tag{102}$$

In these equations, $\lambda(x_3)$ and $\mu(x_3)$ are the Lamé coefficients of the elastic medium (Achenbach 1973), $\rho(x_3)$ is the volume density of mass, while δ_{ij} denotes the Kronecker tensor. Application of the Laplace transformation with respect to time and the 2-D Fourier transformation with respect to the horizontal coordinates brings us to the transform domain. We eliminate the stress components $\hat{\tilde{\tau}}_{i1}$ and $\hat{\tilde{\tau}}_{i2}$, and define the elastic state vector by

$$\hat{\tilde{\mathbf{b}}}_J = \begin{pmatrix} \hat{\tilde{v}}_1 \\ \hat{\tilde{v}}_2 \\ \hat{\tilde{v}}_3 \\ -\hat{\tilde{\tau}}_{13} \\ -\hat{\tilde{\tau}}_{23} \\ -\hat{\tilde{\tau}}_{33} \end{pmatrix}. \tag{103}$$

The differential equation for the elastic state vector is found to be

$$\partial_3 \hat{\tilde{\mathbf{b}}}_I = +s\mathbf{A}_{IJ}(x_3)\hat{\tilde{\mathbf{b}}}_J = \hat{\tilde{\mathbf{u}}}_I, \tag{104}$$

where upper case Latin subscripts range from 1 to 6. The system matrix is found to be

$$\mathbf{A}_{IJ} = \begin{pmatrix} 0 & 0 & -i\alpha_1 & \frac{1}{\mu} & 0 & 0 \\ 0 & 0 & -i\alpha_2 & 0 & \frac{1}{\mu} & 0 \\ -i\xi\alpha_1 & -i\xi\alpha_2 & 0 & 0 & 0 & \frac{1}{\lambda+2\mu} \\ \rho + \beta\alpha_1^2 + \mu\alpha_\eta\alpha_\eta & \beta\alpha_1\alpha_2 & 0 & 0 & 0 & -i\xi\alpha_1 \\ \beta\alpha_1\alpha_2 & \rho + \beta\alpha_2^2 + \mu\alpha_\eta\alpha_\eta & 0 & 0 & 0 & -i\xi\alpha_2 \\ 0 & 0 & \rho & -i\alpha_1 & -i\alpha_2 & 0 \end{pmatrix}, \tag{105}$$

where we have used $\xi = \lambda/(\lambda + 2\mu)$ and $\beta = \mu(3\lambda + 2\mu)/(\lambda + 2\mu)$. For brevity the explicit dependence upon x_3 has been omitted and the subscript notation has been applied, where the lower case Greek symbol η is to be assigned the values 1 and 2. The source strength vector becomes

$$\hat{\tilde{\mathbf{u}}}_I = \delta(x_3 - x_3^S)\begin{pmatrix} \hat{H}_{31}^S + \hat{H}_{13}^S \\ \hat{H}_{32}^S + \hat{H}_{23}^S \\ \xi\hat{H}_{\eta\eta}^S + \hat{H}_{33}^S \\ \hat{F}_1^S + 2i\xi\mu\hat{H}_{\eta\eta}^S\alpha_1 + i\mu(\hat{H}_{\eta 1}^S + \hat{H}_{1\eta}^S)\alpha_\eta \\ \hat{F}_2^S + 2i\xi\mu\hat{H}_{\eta\eta}^S\alpha_2 + i\mu(\hat{H}_{\eta 2}^S + \hat{H}_{2\eta}^S)\alpha_\eta \\ \hat{F}_3^S \end{pmatrix} \tag{106}$$

Next we decompose $\mathbf{A}_{IJ}$ into the product $\mathbf{N}_{IK}\mathbf{\Lambda}_{KL}\mathbf{N}_{LJ}^{-1}$, where $\mathbf{\Lambda}_{KL}$ is a diagonal matrix with the eigenvalues of $\mathbf{A}_{IJ}$, while $\mathbf{N}_{IK}$ is the composition matrix and $\mathbf{N}_{LJ}^{-1}$ is the decomposition matrix. The columns of the composition matrix are the transposed

eigenvectors of $\mathbf{A}_{IJ}$, each multiplied by a normalization factor ϵ_I, i.e.,

$$\mathbf{N}_{IK}=\begin{pmatrix} i\alpha_1\epsilon_1 & i\alpha_1\gamma^S\epsilon_2 & -i\alpha_2\epsilon_3 & i\alpha_1\epsilon_4 & -i\alpha_1\gamma^S\epsilon_5 & -i\alpha_2\epsilon_6 \\ i\alpha_2\epsilon_1 & i\alpha_2\gamma^S\epsilon_2 & i\alpha_1\epsilon_3 & i\alpha_2\epsilon_4 & -i\alpha_2\gamma^S\epsilon_5 & i\alpha_1\epsilon_6 \\ -\gamma^P\epsilon_1 & -\alpha_\eta\alpha_\eta\epsilon_2 & 0 & \gamma^P\epsilon_4 & -\alpha_\eta\alpha_\eta\epsilon_5 & 0 \\ -2i\mu\alpha_1\gamma^P\epsilon_1 & -2i\mu\alpha_1\sigma\epsilon_2 & i\mu\alpha_2\gamma^S\epsilon_3 & 2i\mu\alpha_1\gamma^P\epsilon_4 & -2i\mu\alpha_1\sigma\epsilon_5 & -i\mu\alpha_2\gamma^S\epsilon_6 \\ -2i\mu\alpha_2\gamma^P\epsilon_1 & -2i\mu\alpha_2\sigma\epsilon_2 & -i\mu\alpha_1\gamma^S\epsilon_3 & 2i\mu\alpha_2\gamma^P\epsilon_4 & -2i\mu\alpha_2\sigma\epsilon_5 & -i\mu\alpha_1\gamma^S\epsilon_6 \\ 2\mu\sigma\epsilon_1 & 2\mu\alpha_\eta\alpha_\eta\gamma^S\epsilon_2 & 0 & 2\mu\sigma\epsilon_4 & -2\mu\alpha_\eta\alpha_\eta\gamma^S\epsilon_5 & 0 \end{pmatrix}, \tag{107}$$

where the quantity σ is given by

$$\sigma=\tfrac{1}{2}(\gamma^S)^2-\alpha_\eta\alpha_\eta. \tag{108}$$

The superscripts P and S are used to indicate that the quantity is related P- or compressional waves with wavespeed $c^P=[(\lambda+2\mu)/\rho]^{1/2}$ and S- or shear waves with wavespeed $c^S=(\mu/\rho)^{1/2}$, respectively. Upon substituting $\hat{\mathbf{b}}_I=\mathbf{N}_{IJ}\hat{\mathbf{w}}_J$ in (104), we obtain the system of differential equations for the wave vector $\hat{\mathbf{w}}_J$. When we use the normalization

$$\begin{aligned} &\epsilon_1=\frac{-ic^S}{(2\mu\gamma^P)^{1/2}}, \quad \epsilon_2=\frac{c^S}{(2\mu\alpha_\eta\alpha_\eta\gamma^S)^{1/2}}, \quad \epsilon_3=\frac{1}{(2\mu\alpha_\eta\alpha_\eta\gamma^S)^{1/2}}, \\ &\epsilon_4=\frac{c^S}{(2\mu\gamma^P)^{1/2}}, \quad \epsilon_5=\frac{-ic^S}{(2\mu\alpha_\eta\alpha_\eta\gamma^S)^{1/2}}, \quad \epsilon_6=\frac{-i}{(2\mu\alpha_\eta\alpha_\eta\gamma^S)^{1/2}}, \end{aligned} \tag{109}$$

the total system can be decoupled in two smaller systems.

The first (sub)system involves the wave vector components $\hat{w}_3$ and $\hat{w}_6$ and describes the propagation of the SH- or horizontal shear waves. The eigenvalue matrix is then

$$\mathbf{\Lambda}_{KL}=\begin{pmatrix} -\gamma^S & 0 \\ 0 & \gamma^S \end{pmatrix}, \tag{110}$$

and the coupling matrix is found to be

$$\mathbf{\Delta}^{SH}_{IK}=\begin{pmatrix} 0 & -i\chi^H \\ i\chi^H & 0 \end{pmatrix}, \tag{111}$$

with the inhomogeneity function

$$\chi^H=\frac{1}{2}\left(\frac{\partial_3\gamma^S}{\gamma^S}+\frac{\partial_3\mu}{\mu}\right). \tag{112}$$

The SH system of differential equations strongly resembles the acoustical system described in the main text.

The propagation of the P- and SV-waves, the compressional and vertical shear waves, is described by the other (sub)system of differential equations. The wave vector elements involved are $\hat{w}_1$, $\hat{w}_2$, $\hat{w}_4$ and $\hat{w}_5$. Here the eigenvalue matrix is

$$\mathbf{\Lambda}^{P/SV}_{KL}=\begin{pmatrix} -\gamma^P & 0 & 0 & 0 \\ 0 & -\gamma^S & 0 & 0 \\ 0 & 0 & \gamma^P & 0 \\ 0 & 0 & 0 & \gamma^S \end{pmatrix}. \tag{113}$$

The coupling matrix is more complex now and is given by

$$\mathbf{\Delta}^{P/SV}_{IK}=\begin{pmatrix} 0 & -i\chi^T & -i\chi^P & -\chi^R \\ i\chi^T & 0 & \chi^R & -i\chi^S \\ i\chi^P & -\chi^R & 0 & -i\chi^T \\ \chi^R & i\chi^S & i\chi^T & 0 \end{pmatrix}, \tag{114}$$

where we have used the inhomogeneity functions

$$\chi^T=\left(\frac{\alpha_\eta\alpha_\eta}{\gamma^S\gamma^P}\right)^{1/2}\left[(c^S)^2(\alpha_\eta\alpha_\eta-\gamma^S\gamma^P)\frac{\partial_3\mu}{\mu}+\frac{\partial_3\rho}{2\rho}\right], \tag{115}$$

$$\chi^R=\left(\frac{\alpha_\eta\alpha_\eta}{\gamma^S\gamma^P}\right)^{1/2}\left[(c^S)^2(\alpha_\eta\alpha_\eta+\gamma^S\gamma^P)\frac{\partial_3\mu}{\mu}+\frac{\partial_3\rho}{2\rho}\right], \tag{116}$$

$$\chi^P = \frac{1}{2}\left[4(c^S)^2\alpha_\eta\alpha_\eta\frac{\partial_3\mu}{\mu} - \frac{\partial_3\gamma^P}{\gamma^P} + \frac{\partial_3\rho}{\rho}\right], \tag{117}$$

$$\chi^S = \frac{1}{2}\left[-4(c^S)^2\alpha_\eta\alpha_\eta\frac{\partial_3\mu}{\mu} + \frac{\partial_3\gamma^S}{\gamma^S} - \frac{\partial_3\rho}{\rho}\right]. \tag{118}$$

Now not only a coupling between the up- and downgoing parts of the P- and SV-waves takes place, but also between the P- and SV-waves. This means that, unlike the SH-waves, conversion between P- and SV-waves is possible. When this takes place, of course also the wavespeed and the propagation factor of vertical slowness change.

Having derived the systems of differential equations for the SH- and the P/SV-wave vector components, the remaining steps are straightfoward. Both for the SH case and for the P/SV case the Neumann scheme or WKBJ iterative solution remains a valid tool for finding the transform-domain wave vector, although it is inevitable that the scheme becomes more elaborate in the latter case, due to the coupling between P- and SV-waves. Once the WKBJ iterative solution has been found, we can construct the total wave vector, and its components can be multiplied by the appropriate composition matrix $\mathbf{N}_{IJ}$ (at this stage singularities, introduced by the normalization, can be proved to have no effect). The resulting components can be transformed back to the space–time domain using the modified Cagniard method. Here the P–SV conversion can also cause some inconvenience by making both γ^S and γ^P play a role in the determination of the modified Cagniard contour, but this problem is not fundamental. Finally, we remark that not only the *method* of this paper turns out to be applicable to wave propagation in elastic media, but also the *conclusions* connected to this method remain valid in this case.

APPENDIX D: ELIMINATION OF POLES FROM HIGHER ORDER WAVE COMPONENTS

From equation (70) in Section 7 it can be inferred that the inhomogeneity function $\tilde{\chi}(x_3)$ has a pair of poles that always coincide with two branch points in the complex p-plane, one of which is in the right half of this plane. Also we know that the modified Cagniard contour can reach the latter branch point, in which case we must make a detour around it. As a consequence, the residue of this branch point sometimes shows up in the modified Cagniard method. For higher order wave components, the number of poles introduced by the inhomogeneity function in the right half plane equals the order, while some or all of them can coalesce. Advancing along the lines of Section 7, the modified Cagniard method can also be used for the inversion of wave components of order two and higher.

However, the numerical evaluation of the resulting integrals can be difficult, especially when multiple poles are present. For this reason it can be attractive to derive an expression from which these poles of the inhomogenity function have been eliminated, so the singularities in the complex p-plane are common branch points only. To illustrate how this is done, we take the general first-order transform-domain Green's function $\hat{\tilde{G}}^{(1)-}$ [compare equation (42), second term]:

$$\hat{\tilde{G}}^{(1)-} = \int_M^\infty \Pi\chi(x_3)\exp\left[-s\left(\int_{x_3^S}^{x_3} + \int_{x_3^R}^{x_3}\right)\gamma\,d\zeta\right]dx_3. \tag{119}$$

When we look at the inhomogeneity function

$$\chi(x_3) = \frac{\partial_3 Y(x_3)}{2Y(x_3)} = \tfrac{1}{2}\,\partial_3 \ln\gamma(x_3) - \tfrac{1}{2}\,\partial_3 \ln\rho(x_3) = \frac{-\partial_3 c(x_3)}{2c^3(x_3)\gamma^2(x_3)} - \frac{\partial_3\rho(x_3)}{2\rho(x_3)}, \tag{120}$$

we see that although $\hat{\tilde{G}}^{(1)-}$ consists of two terms, only one of them gives rise to a pole; it will therefore be called $\hat{\tilde{G}}^{(1)-}_{\text{pole}}$. We are only interested in this term; it can be written as

$$\hat{\tilde{G}}^{(1)-}_{\text{pole}} = \frac{1}{2}\int_M^\infty \Pi[\partial_3 \ln\gamma(x_3)]\exp\left[-s\left(\int_{x_3^S}^{x_3} + \int_{x_3^R}^{x_3}\right)\gamma\,d\zeta\right]dx_3. \tag{121}$$

Carrying out an integration by parts yields

$$\hat{\tilde{G}}^{(1)-}_{\text{pole}} = -\tfrac{1}{2}\Pi \ln\gamma(M)\exp\left[-s\left(\int_{x_3^S}^{M} + \int_{x_3^R}^{M}\right)\gamma\,d\zeta\right] + s\int_M^\infty \Pi\gamma(x_3)\ln\gamma(x_3)\exp\left[-s\left(\int_{x_3^S}^{x_3} + \int_{x_3^R}^{x_3}\right)\gamma\,d\zeta\right]dx_3, \tag{122}$$

where the principal branch of the logarithmic function is understood. We have now obtained an expression with no poles of the inhomogeneity function incorporated. In an equivalent manner multiple poles in higher order wave components can be eliminated by repeated integration by parts. This means we no longer have to worry about the addition of an extra residual term, thus reducing the organizational overhead. However, the splitting of the Green's function in several terms, some of them preceeded by a positive power of the Laplace transform parameter s, means that the last step of the modified Cagniard method, the convolution with the source signature, becomes more complicated.